

DOKUZ EYLÜL UNIVERSITY
GRADUATE SCHOOL OF NATURAL AND APPLIED SCIENCES

**DESIGN AND IMPLEMENTATION OF
DIELECTRIC RESONATOR BASED
METAMATERIALS**

by
Gizem KALENDER

July, 2015
İZMİR

DESIGN AND IMPLEMENTATION OF DIELECTRIC RESONATOR BASED METAMATERIALS

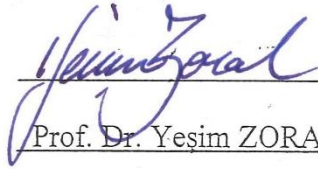
**A Thesis Submitted to the
Graduate School of Natural and Applied Sciences of Dokuz Eylül University
In Partial Fulfillment of the Requirements for the Degree of Master of Science
in Electrical and Electronics Engineering Program**

**by
Gizem KALENDER**

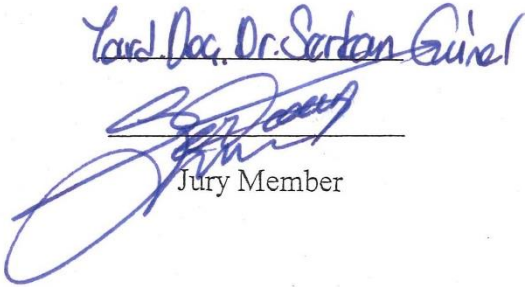
**July, 2015
İZMİR**

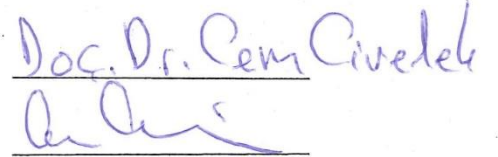
M.Sc THESIS EXAMINATION RESULT FORM

We have read the thesis entitled “**DESIGN AND IMPLEMENTATION OF DIELECTRIC RESONATOR BASED METAMATERIALS**” completed by **GİZEM KALENDER** under supervision of **PROF. DR. YEŞİM ZORAL** and we certify that in our opinion it is fully adequate, in scope and in quality, as a thesis for degree of Master of Science.


Prof. Dr. Yeşim ZORAL

Supervisor


Prof. Dr. Serkan Günel
Jury Member


Prof. Dr. Cem Civelek
Jury Member



Prof. Dr. Ayşe OKUR

Director

Graduate School of Natural and Applied Sciences

ACKNOWLEDGEMENTS

I would like to express my deepest gratitude to my supervisor, Prof. Dr. Yeřim Zoral, for her invaluable guidance, suggestions and support through my thesis. I greatly appreciate her guidance in every part of my graduate education.

I would also like to thank to Assoc. Prof. Dr. Mustafa Seęmen, for invaluable comments and suggestions which improved the quality of the thesis.

I am also very grateful to my parents and also to my sister for their love and encouragement.

I also would like to thank to my dear friends Burcu Babaoęlan, Gönöl Bięil, Nursima Kőroęlu for their support and friendship.

Gizem KALENDER

DESIGN AND IMPLEMENTATION OF DIELECTRIC RESONATOR BASED METAMATERIALS

ABSTRACT

In this thesis, a metamaterial structure based on an array of dielectric resonators is designed and implemented in waveguides. In the first part of this thesis, the metamaterial characteristics of an array containing dielectric resonators is demonstrated by evaluating the permittivity and permeability of the array structure in rectangular waveguide and parallel-plate waveguide at X-band. The scattering parameters in both structures are obtained with CST Microwave Studio simulations and supported with measurement results. Then, the effective relative permittivity and permeability values are extracted with the de-embedding technique and retrieval method, and the frequencies at which the structures possess both negative permeability and negative permittivity simultaneously are shown. It is shown that the array with dielectric resonators has metamaterial characteristics at certain frequency bands. In addition, these certain frequencies of both structures are found to be consistent to each other. This means that the metamaterial behaviour of the dielectric resonator array is highly insensitive to the wave excitation. In the second part of the thesis, an implementation of the metamaterial structure is used in a waveguide directional coupler. For this purpose, a four-hole waveguide directional coupler in X-band is designed. Then, the block of dielectric-resonator array is inserted between isolation port and holes of the coupler, and the performances of the coupler with and without dielectric resonators are compared in terms of the coupling and isolation. The obtained results show that the coupler with dielectric resonators significantly improves the coupling and isolation performances at a new operation frequency band at which the traditional coupler does not work. Therefore, the metamaterial structure attains multi-band characteristics to the coupler. Besides, this new frequency band can be shifted by arranging the distance between the dielectric resonators and holes. Finally, it is also observed that the bandwidth of the new frequency band can be increased by using more dielectric resonators in the array.

Keywords: Metamaterials, dielectric resonators, effective medium parameter extraction, waveguide, scattering parameters.

DİELEKTRİK REZONATÖR TABANLI METAMALZEMELERİN TASARIM VE UYGULAMASI

ÖZ

Bu tezde, bir dielektrik rezonatör dizisine dayanan bir metamalzeme yapısı tasarlanmış ve bu yapının dalga kılavuzlarındaki uygulamaları gerçekleştirilmiştir. Bu tezin ilk kısmında, X-banttaki dikdörtgen dalga kılavuzu ve paralel düzlem dalga kılavuzu içindeki dizi yapısının elektriksel ve manyetik geçirgenliği hesaplanarak dielektrik rezonatörler içeren bir dizinin metamalzeme karakteristiği gösterilmiştir. Her iki yapının da saçılım parametreleri CST Microwave Studio benzetim programları ile çıkarılmış ve ölçüm sonuçları ile desteklenmiştir. Daha sonra gömülü kısımların çıkartılması tekniği ve parametre çıkarma yöntemi ile yapıların etkin göreceli elektrik and manyetik geçirgenlik değerleri elde çıkartılmış ve yapıların hangi frekanslarda aynı anda hem negatif elektriksel geçirgenlik hem de negatif manyetik geçirgenliği sahip oldukları gösterilmiştir. Böylece dielektrik rezonatörlü dizinin belli frekans bantlarında metamalzeme karakteristiğine sahip olduğu gösterilmiştir. Ayrıca, her iki yapıya ait bu belli frekansların birbirine yakın olduğu bulunmuştur. Bu anlamda, dielektrik rezonatör dizisinin metamalzeme karakteristiğinin dalga uyarımına hassas olmadığı gösterilmiştir. İkinci kısmında, bahsedilen yapının bir yönlü dalga kılavuzu kuplörü üzerindeki uygulaması gerçekleştirilmiştir. Bu amaçla X bantta dört delikli bir yönlü dalga kılavuzu kuplörü tasarlanmıştır. Daha sonra dielektrik rezonatör dizisi bloğu, kuplörün yalıtım kapısı ve delikleri arasına yerleştirilmiştir ve dielektrik rezonatörlü olan ve olmayan kuplörün performansları kuplaj ve yalıtım açısından karşılaştırılmıştır. Dielektrik rezonatörlü kuplör, geleneksel kuplörün çalışmadığı yeni bir frekans bandındaki kuplaj ve yalıtım performanslarını ciddi bir biçimde iyileştirmiştir. Böylece yapıya metamalzeme eklenmesi kuplöre çoklu bant karakteristiği kazandırmıştır. Ayrıca bu yeni frekans bandı, dielektrik rezonatörler ve delikler arasındaki mesafe ayarlanarak kaydırılabilir. Yeni frekans bandının bant genişliğinin dizide daha fazla dielektrik rezonatör kullanarak arttırılmıştır.

Anahtar kelimeler: Metamalzemeler, dielektrik rezonatörler, etkin ortam parametre çıkarımı, dalga kılavuzu, saçılım parametreleri.

CONTENTS

	Page
M.Sc THESIS EXAMINATION RESULT FORM.....	ii
ACKNOWLEDGEMENTS	iii
ABSTRACT.....	iv
ÖZ	v
LIST OF FIGURES	viii
LIST OF TABLES	xi
 CHAPTER ONE-INTRODUCTION	 1
 1.1 Aim of the Thesis	 2
1.2 Thesis Outline.....	3
 CHAPTER TWO-THEORY AND APPLICATIONS OF METAMATERIALS	 4
 2.1 Definition of Metamaterials	 4
2.2 Properties of Metamaterials.....	5
2.2.1 Negative Permittivity.....	7
2.2.2 Negative Permeability.....	8
2.2.3 Negative Refraction Index.....	9
2.3 Examples of Metamaterial Structures	11
2.3.1 Split Ring Resonators	11
2.3.2 Dielectric Resonators Based Metamaterials	13
2.4 Applications of Metamaterials	15
2.4.1 Frequency Selective Surface Based Metamaterial.....	15
2.4.2 Metamaterial Antennas.....	16
2.4.3 Metamaterial Power Divider and Coupler.....	18
2.4.4 Metamaterial Clocking Devices.....	19
2.4.5 Superlens.....	20

CHAPTER THREE-DIELECTRIC RESONATOR BASED METAMATERIAL STRUCTURE	22
3.1 De-embedding Processes.....	23
3.2 Retrieval Technique	26
3.3 The Structure (In Rectangular Waveguide and Parallel Plate Waveguide)	29
3.3.1 The Results of Waveguide Structure	31
3.3.2 Results of Parallel-Plate Waveguide Structure.....	35
 CHAPTER FOUR-APPLICATION OF DIELECTRIC RESONATOR BASED METAMATERIAL STRUCTURE IN WAVEGUIDE COUPLER	 39
4.1 Theory of Multihole Waveguide Coupler	39
4.2 Performance Analysis of Coupling and Isolation with Metamaterial Structure41	
 CHAPTER FIVE-CONCLUSION	 53
 REFERENCES.....	 56
 APPENDICES	 62

LIST OF FIGURES

	Page
Figure 2.1	Medium classification of materials. 4
Figure 2.2	(a) Right-handed orthogonal coordinate system (b) Left-handed orthogonal coordinate system. 6
Figure 2.3	A periodic thin wire. 7
Figure 2.4	Examples of different shapes of resonators. a) split ring resonator (SRR) b) the spiral resonator (SR) c) labyrinth resonator d) the U- shaped resonator (USR). 8
Figure 2.5	Reflection and refraction of an incident wave through a boundary of two different media. 9
Figure 2.6	Refraction in the left-hand and right hand media. 11
Figure 2.7	a) The periodic structures of SRR b) Thin metallic wires. 12
Figure 2.8	A periodic array of thin wires and SRRs. 12
Figure 2.9	Excitation types a) Magnetic excitation b) Electric and magnetic excitation 13
Figure 2.10	Some dielectric resonators. 14
Figure 2.11	Array of dielectric resonators having negative permeability and negative permittivity unit cells. 14
Figure 2.12	Dielectric resonator metamaterials in parallel plate waveguide. 15
Figure 2.13	The loop wire metamaterial based FSS. 16
Figure 2.14	An example of metamaterial antenna. 17
Figure 2.15	An example of metamaterial antenna with dielectric resonator. 17
Figure 2.16	A metamaterial based power divider. 18
Figure 2.17	Metamaterial based (left) and traditional (right) microstrip directional coupler. 19
Figure 2.18	Invisible objects. 20
Figure 2.19	Refraction of wave in the metamaterial medium. 21
Figure 3.1	The schematic for de-embedding process. 23
Figure 3.2	A two-port transmission line 24

Figure 3.3	(a) Simulation view and (b) photograph of structure.	30
Figure 3.4	The experimental setup for two DRs within the waveguide structure.	31
Figure 3.5	(a) S_{11} (dB) and (b) S_{21} (dB) of the two dielectric resonator array within the rectangular waveguide structure.....	32
Figure 3.6	(a) Effective permittivity and (b) permeability of the structure for the rectangular waveguide.....	34
Figure 3.7	(a) S_{11} (dB) and (b) S_{21} (dB) the two dielectric resonator array in parallel-plate waveguide.....	36
Figure 3.8	(a) Effective permittivity and (b) Effective permeability for parallel-plate waveguide.	37
Figure 4.1	A typical Bethe hole directional coupler.	39
Figure 4.2	Working mechanism of two-hole coupler.	41
Figure 4.3	Simulation view of four-hole coupler.....	42
Figure 4.4	Coupling and isolation of multihole coupler without dielectric resonators.....	43
Figure 4.5	Simulation view of four-hole coupler with two dielectric resonators.....	44
Figure 4.6	The coupling and the isolation of multihole coupler with two dielectric resonators.....	44
Figure 4.7	Coupling of multihole coupler with and without two dielectric resonators.....	46
Figure 4.8	Isolation of multihole coupler with and without two dielectric resonators.....	46
Figure 4.9	Simulation view of four-hole coupler with three dielectric resonators.	47
Figure 4.10	Coupling of multihole coupler with three dielectric resonators with different distances from holes.	47
Figure 4.11	Isolation of multihole coupler with three dielectric resonators with different distances from holes.	48
Figure 4.12	Coupling of multihole coupler with different number of dielectric resonators.....	51

Figure 4.13 Isolation of multihole coupler with different number of dielectric resonators.....	52
--	----

LIST OF TABLES

	Page
Table 2.1 Sign of index of refraction.	10
Table 3.1 Comparision of the negative values of ϵ and μ in rectangular waveguide and parallel plate waveguide.	38

CHAPTER ONE

INTRODUCTION

Electromagnetic waves have important role, since they carry energy and information from one point to another point without any physical connection between the points. Electromagnetic waves can travel through air, solid materials, and vacuum. Propagation of electromagnetic waves depends on properties of materials. These properties are defined by permittivity (ϵ) and permeability (μ). Permittivity is defined as resistance of the material with respect to electric field. While the permittivity describes how much electric field is produced per unit in the medium, the permeability is a constant that exists between magnetic field intensity and magnetic induction. It is also called magnetic permeability.

Materials in the nature have positive values ϵ and μ . In 1968, artificial medium that have negative values of ϵ and μ was proposed by Dr. Victor Veselago (Veselago, 1968). Artificial materials that have these properties are called as metamaterials. Metamaterials provide negative refraction, backward propagation, and reverse doppler effect not common in nature. Also, these materials are called as left-handed (LH) materials or double negative (DNG) materials. When the signs of ϵ and μ in the Maxwell's equations are changed, one get a left-handed triplet. After the theoretical proposal of Victor Veselago, almost 30 years later, in 1996, John B. Pendry suggested a periodic array of copper wires having certain radius with negative ϵ in certain frequency band. In 1999, he also suggested that an electromagnetic response of negative μ is produced with a periodic array of split ring resonators (Pendry, Holden, Stewart, & Youngs, 1996; Pendry, Holden, Robbins, & Stewart, 1999; Pendry, 2000). In order to construct a structure with both negative ϵ and μ , periodic arrays of copper wires and split ring resonators are required. David Smith proposed the composite which is a metamaterial with both negative ϵ and μ (Smith, & Kroll, 2000). Later, various types of structure and application related to metamaterial followed these studies.

In recent years, there has been significant increase in the number of research related to the metamaterial structures in several applications such as antennas, sensors, filters, absorbers etc. It is shown that, using the metamaterials that have unusual response to the presence of electromagnetic fields, the new kind compact size microwave components and antennas can be created for communication applications.

Metamaterial based antenna has been designed in order to enhance antenna gain and beamwidth. Also metamaterial antennas can provide compact size (Chen, & Alu, 2010; Majadi, & Atari, 2013; Kim, & Varadan, 2010; Sahu, Tripathi, & Singh, 2013). The investigation about the fundamental properties of the negative index metamaterials (Smith, & Kroll, 2000; Smith, & Pendry, 2004) and the researches related to extractions of effective medium parameter (Ghodgaonkar, Varadan, & Varadan, 1990; Smith, Vier, Koschny, & Soukoulis, 2005; Smith, & Larauche, 2010; Weir, 1974) are studied. Metamaterial sensors, frequency tunable metamaterial structures, perfect lens (Pendry, 2000; Yang, Huang, Tang, Zeng, & Dong, 2013; Aydin, & Özbay, 2007; Aydin, Bulu, & Ozbay, 2007) are some of the applications related to metamaterial.

1.1 Aim of the Thesis

The study in this thesis is mainly aimed to the implementation of dielectric resonator based metamaterial in waveguide structures, and use this structure in an application, which is improvement of the performance of waveguide multihole coupler. Although the dielectric resonator based metamaterials are mentioned and discussed in the literature, the corresponding studies are mainly for free-space structures. There exists a few studies about dielectric resonator based metamaterials in waveguide structure; however, they neither include an analysis about the extraction of medium parameters whose results can validate the material being a metamaterial nor propose an application of this metamaterial in a waveguide structure. An array of dielectric resonator placed in a WR90 waveguide is proposed as a metamaterial structure and the effective permittivity and the effective

permeability of the suggested structure is derived. It is shown that the dielectric resonator array placed in a waveguide shows metamaterial characteristics at certain frequencies. After the validation of the metamaterial characteristics of the structure, this metamaterial is implemented in waveguide multihole coupler. According to the results, it is observed that both coupling and isolation performances of the coupler with dielectric resonators are improved by adding a new band (multi-band) to the operating frequency band of the traditional coupler (coupler without metamaterial).

1.2 Thesis Outline

The thesis includes five chapters, and the outline of the thesis is given as follows. Chapter 1 gives a brief introduction about the metamaterials, and the aim of the study realized in this thesis.

Chapter 2 explains the background knowledge about metamaterials including historical development and material properties of the metamaterials. Furthermore, some well-known examples and applications of the metamaterials are given in this Chapter.

In Chapter 3, a realization of a study about dielectric resonator based metamaterial is presented. Here, the rectangular waveguide and parallel-plate waveguide structures in which an array of dielectric resonators is embedded are described. Then, the corresponding simulation and measurement results are demonstrated by including the extraction of effective medium parameters, and the discussion about the results is given.

Chapter 4 consists of an extension study to the one in Chapter 3, which is the insertion of dielectric resonator array into the waveguide multihole coupler. In this application, the performance improvement of coupling and isolation of the multihole coupler with the dielectric resonator metamaterial is analyzed and discussed.

The conclusions and suggestions for future works are presented in Chapter 5.

CHAPTER TWO

THEORY AND APPLICATIONS OF METAMATERIALS

2.1 Definition of Metamaterials

The response of materials in presence of electromagnetic field is determined by parameters known as magnetic permeability (μ) and electric permittivity (ϵ). These parameters have positive value for material in nature. According to the sign of permittivity ϵ and permeability μ , the classification of different media can be made as depicted in Figure 2.1. Negative values of ϵ and μ can be obtained by artificial structures.

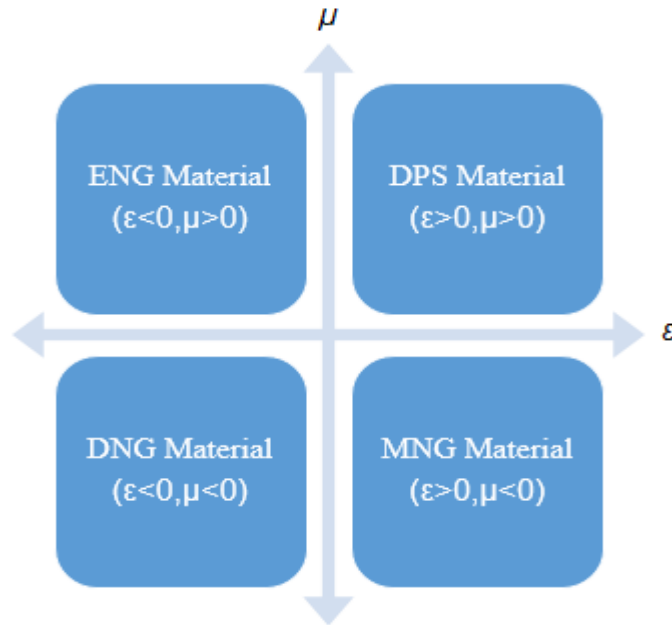


Figure 2.1 Medium classification of materials.

Double positive (DPS) medium is the one with both positive permittivity and permeability. Generally, materials in nature fall under this region. Epsilon-negative (ENG) medium is a medium with negative permittivity and positive permeability. This characteristic is observed in many plasmas at some specific frequency regions. Mu-negative medium (MNG) is defined medium with positive permittivity and negative permeability. Specific examples for this region are gyrotropic materials (Engheta, & Ziolkowski, 2006). Double negative (DNG) medium is a designed

medium with both negative permittivity and permeability. Double negative materials are also called metamaterials, or negative index material (NIM) or Left-handed (LH) materials.

2.2 Properties of Metamaterials

Almost all materials encountered in nature follow right hand rule. Namely, the materials that have their permeability and permittivity greater than zero can be defined by using right-hand triplet.

The electric field intensity (\vec{E}), magnetic field intensity (\vec{H}) and propagation vector (\vec{k}) obey right hand rule. The cross product in respect to a right handed coordinate system is shown in Figure 2.2(a). The electric field intensity vector (\vec{E}), is in the positive x direction, the magnetic field intensity vector (\vec{H}) is in the positive y direction, and the wave propagates in the positive z direction. The curls of these vectors are according to Faraday's law and Ampere law, are given in equations (2.1) and (2.2) for a lossless ($\sigma=0$) medium. The equations (2.3) and (2.4) define constitutive relations in a simple medium (i.e. homogeneous, linear, isotropic and non-dispersive medium).

$$\vec{\nabla} \times \vec{H} = \frac{\partial \vec{D}}{\partial t} \quad (2.1)$$

$$\vec{\nabla} \times \vec{E} = -\frac{\partial \vec{B}}{\partial t} \quad (2.2)$$

$$\vec{B} = \mu \vec{H} = \mu_0 \mu_r \vec{H} \quad (2.3)$$

$$\vec{D} = \epsilon \vec{E} = \epsilon_0 \epsilon_r \vec{E} \quad (2.4)$$

where \vec{D} is the electric flux density, \vec{B} is the magnetic flux density vectors, and also

$\epsilon_0 = 8.854 \times 10^{-12}$ F/m is the permittivity of the free space, $\mu_0 = 4\pi \times 10^{-7}$ H/m is the permeability of the free space, ϵ_r and μ_r are the relative permittivity and the permeability of the medium, respectively.

These laws can be expressed in phasor domain for monochromatic plane wave using $e^{j\omega t}$ convention;

$$\bar{k} \times \bar{E} = \omega \mu \bar{H} \quad (2.5)$$

$$\bar{k} \times \bar{H} = -\omega \epsilon \bar{E} \quad (2.6)$$

If both ϵ and μ are positive in equation (2.5) and (2.6), this implies that the vectors \bar{E} , \bar{H} and \bar{k} obey right hand rule. If both ϵ and μ have negative values, then the vectors \bar{E} , \bar{H} and \bar{k} obey left hand rule. The directions of these vectors fields are shown in Figure 2.2 (b).

The complex Poynting vector (\bar{S}), a power density vector related with an electromagnetic field is given by

$$\bar{S} = \bar{E} \times \bar{H}^* \quad (2.7)$$

where \bar{H}^* is the complex conjugate of magnetic field intensity vector. Poynting vector \bar{S} has the same direction as the propagation vector \bar{k} in right hand materials. However, Poynting vector \bar{S} is in the opposite direction of the propagation vector \bar{S} in left-handed materials.

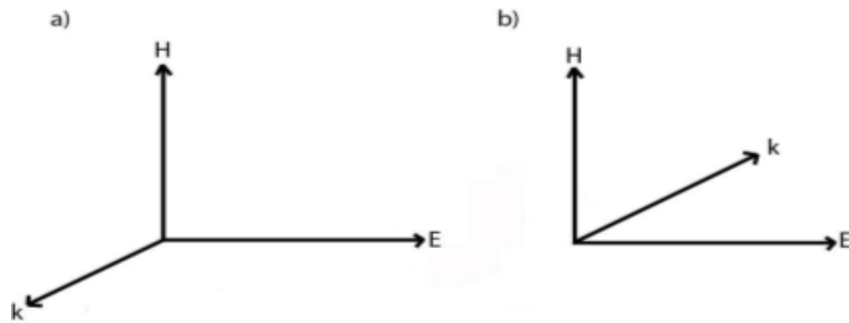


Figure 2.2 (a) Right-handed orthogonal coordinate system (b) Left-handed orthogonal coordinate system.

2.2.1 Negative Permittivity

Some metals behave like a plasma of free electrons. Negative permittivity can be provided under a specific frequency called plasma frequency (Ekmekçi, 2010; Pendry et al., 1999). The negative dielectric permittivity is dominant in visible light and ultraviolet light frequencies due to the plasma frequency of metals in optical frequencies. To obtain negative permittivity in microwave spectrum, a periodic array of metallic thin wires are utilized (Ekmekçi, 2010; Pendry et al., 1999). The permittivity function in metals is formulated as

$$\epsilon_{metal}(\omega) = 1 - \frac{\omega_p^2}{\omega^2} \quad (2.8)$$

where ω_p is plasma frequency. The plasma frequency of the metallic thin wire is formulated as

$$\omega_p = \frac{ne^2}{\epsilon_0 m} = \frac{2\pi c_0^2}{a^2 \ln(a/r)} \quad (2.9)$$

where n is the electron density, m is the mass of the electron, e is the charge of an electron, c_0 is the speed of light in vacuum, a is lattice parameter, and r is the radius of the cylindrical thin wires (Ekmekçi, 2010; Pendry et al., 1999). For the metallic thin wire, the medium can be described as in Figure 2.3. The structure having negative permittivity values can be realized by adjusting the appropriate parameters such as r and a given above.

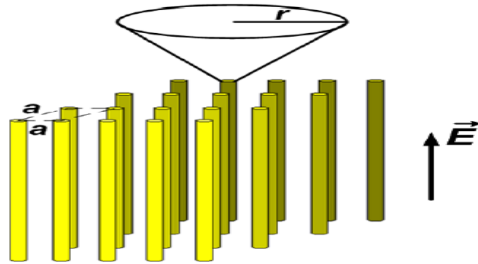


Figure 2.3 A periodic thin wire (Ekmekçi, 2010)

When the separation between metallic thin wires (a) are structured less than the wavelength (λ) of the incident wave ($a \ll \lambda$), the response of the system can be treated by way of the effective medium theory (Koschny, 2004), which includes the effective electric permittivity ϵ_{eff} and the magnetic permeability μ_{eff} of the medium.

2.2.2 Negative Permeability

Due to the lack of free magnetic charges in nature, obtaining a material with negative permeability is much more difficult than designing a material with negative dielectric permittivity. The negative permeability can not be obtained by using the thin wire arrays. Magnetic resonator structures suggested by Pendry et. al are the only means to obtain materials with negative permeability (Pendry et al., 1999). The structures are periodic arrays in order to couple each other and to obtain strong magnetic response that gives rise to negative permeability. Magnetic dipole moment can be created by using a current carrying conductor loop. The most common magnetic resonator structures are the split ring resonator (SRR), spiral resonator, U-shaped resonator, (Ekmekçi, 2010). The examples of these structures are showed in Figure 2.4.

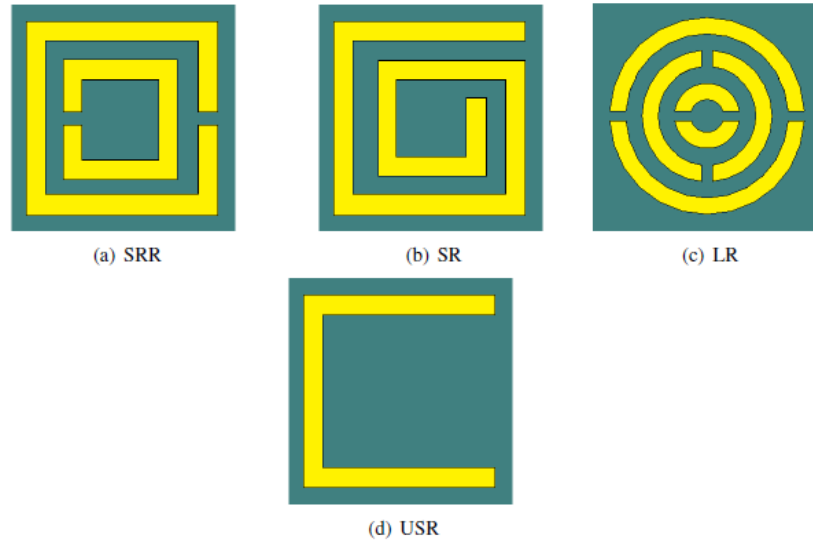


Figure 2.4 Examples of different shapes of resonators. a) split ring resonator (SRR) b) the spiral resonator (SR) c) labyrinth resonator d) the U-shaped resonator (USR) (Ekmekçi, 2010).

2.2.3 Negative Refraction Index

The refractive index (n) of an optical medium explains the ratio of speed of light to phase velocity of the medium. As shown in Figure 2.5, Snell's law of reflection states that the relationship between the incident angle and refracted angle. It is given as

$$\frac{\sin \theta_1}{\sin \theta_2} = \frac{n_2}{n_1} = \sqrt{\frac{\mu_2 \epsilon_2}{\mu_1 \epsilon_1}} \quad (2.10)$$

where θ_1 is incident angle with surface normal, θ_2 is the transmitted angle, n_1 and n_2 are the refractive indices of medium 1 and 2, respectively.

However, if one of the media is left handed, the equation (2.10) is modified to

$$\frac{\sin \theta_1}{\sin \theta_2} = \frac{n_2}{n_1} = \frac{p_2}{p_1} \sqrt{\frac{\mu_2 \epsilon_2}{\mu_1 \epsilon_1}} \quad (2.11)$$

where p_1 is set to be constant value of +1 if medium 1 is right handed, and -1 if medium 1 is left handed. In a similar way, setting the values of p_2 as +1 or -1, the medium can be modeled as right handed or left handed (Engheta, & Ziolkowski, 2006).

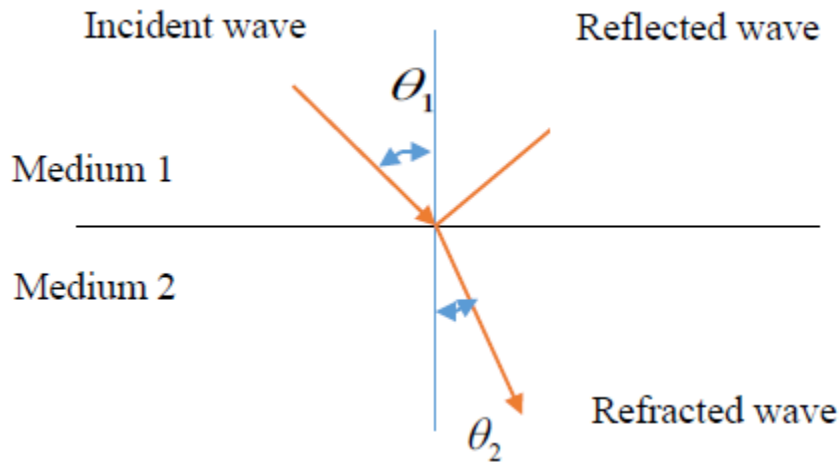


Figure 2.5 Reflection and refraction of an incident wave through a boundary of two different media.

The sign of index of refraction is given in Table 2.1. In this table, n is the refraction index, $j=\sqrt{-1}$ is imaginary unit. Since $n=\sqrt{\epsilon_r\mu_r}$;

- When $\epsilon_r > 0$ and $\mu_r > 0$, $n=[|\epsilon_r|e^{j0}|\mu_r|e^{j0}]^{1/2} = |\epsilon_r||\mu_r|e^{j0}=|\epsilon_r||\mu_r|$ which is a positive number.
- When $\epsilon_r > 0$ and $\mu_r < 0$, $n=[|\epsilon_r|e^{j0}|\mu_r|e^{j\pi}]^{1/2} = j|\epsilon_r||\mu_r|e^{j\pi/2}=|\epsilon_r||\mu_r|$ which is a purely imaginary number.
- When $\epsilon_r < 0$ and $\mu_r > 0$, $n=[|\epsilon_r|e^{j\pi}|\mu_r|e^{j0}]^{1/2} = j|\epsilon_r||\mu_r|e^{j\pi/2}=|\epsilon_r||\mu_r|$ which is a purely imaginary number.
- When $\epsilon_r < 0$ and $\mu_r < 0$, $n=[|\epsilon_r|e^{j\pi}|\mu_r|e^{j\pi}]^{1/2} = |\epsilon_r||\mu_r|e^{j\pi}=-|\epsilon_r||\mu_r|$ which is a negative number.

Table 2.1 Sign of index of refraction.

n	$\epsilon_r > 0$	$\epsilon_r < 0$
$\mu_r > 0$	+	j
$\mu_r < 0$	j	-

When the refraction index is less than zero, the refracted angle should have a negative value. In this case, the refracted wave propagates to backward direction, staying on the same half plane with the incident wave. Negative refraction and positive refraction are shown as Figure 2.6. If refraction index is greater than zero, then refracted wave propagates to forward direction.

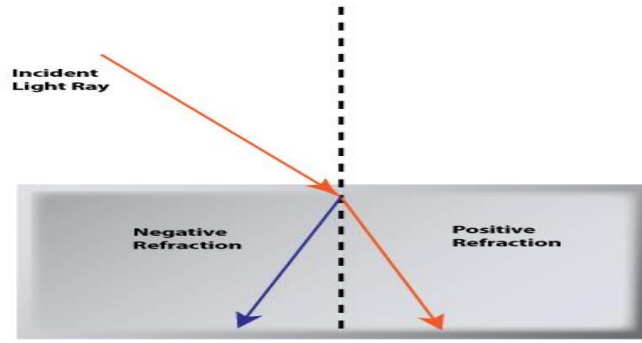


Figure 2.6 Refraction in the left-hand and right hand media.

2.3 Examples of Metamaterial Structures

2.3.1 Split Ring Resonators

Split ring resonators (SRRs) are the most common metamaterial resonator structures. The schematic view of the common SRR structure and thin wires are given in Figure 2.7 (Withayachumnankul, & Abbott, 2009). SRRs have two concentric annular rings having splits in them at opposite ends. The splits and gaps in the SRR structures are capacitive elements in obtaining magnetic resonance. The periodic arrangements of SRRs array (increasing in the number of SRRs) given in the Figure 2.7(a) make a significant increase in magnetic resonance due to coupling between SRRs. This fact creates a negative permeability during the resonance band. While the copper loops change the magnetic response, thin wires on the surface behind provide the required electrical response. The periodic array of thin metallic wires in Figure 2.7(b) creates negative real part of dielectric permittivity during the resonance band. The periodic structure of SRRs and thin wires is shown as Figure 2.8.

The parameters such as unit cell size (a), width of the gap (d), width of the metal strips (c) and separation distance between the neighbouring ring (l) of SRR in Figure 2.7(a) affect the resonance frequency of the structure which is frequently studied in literature (Smith, & Kroll, 2000; Withayachumnankul, & Abbott, 2009; Garcia et al., 2005; Markos, & Soukoulis, 2001; Ekmekçi, & Turhan-Sayan, 2009). The electrical and magnetic behaviours of the SRR structure at this resonance frequency depend on

technique of excitation. These excitation techniques are electrical excitation, magnetic excitation and both electrical and magnetic excitation which are depicted in Figure 2.9 (Ekmekçi, 2010).

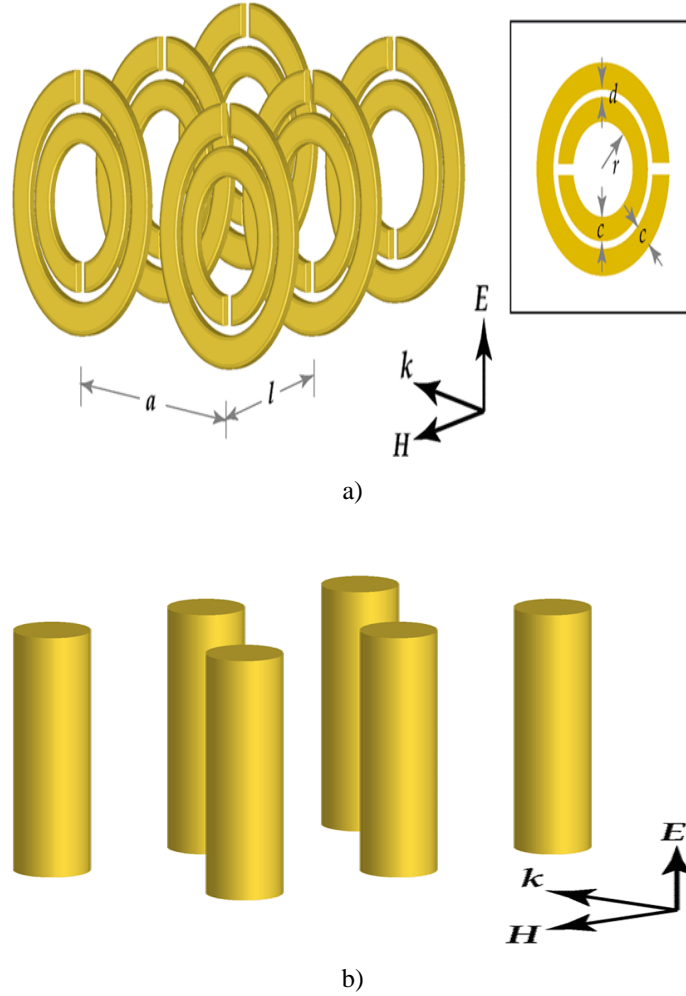


Figure 2.7 a) The periodic structures of SRR b) Thin metallic wires (Withayachumnankul & Abbott, 2009).

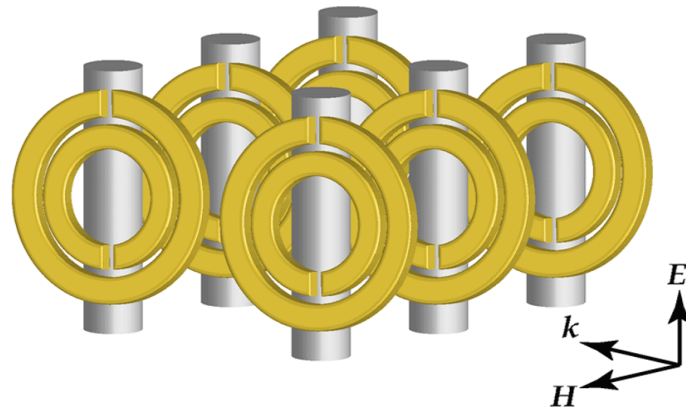


Figure 2.8 A periodic array of thin wires and SRRs (Withayachumnankul & Abbott, 2009).

The magnetic excitation can be only achieved when the magnetic field intensity (\vec{H}) is perpendicular to the loops in SRR due to the Faraday's law of induction. On the other hand, electric excitation is achieved when the electric field intensity (\vec{E}) is parallel to the gaps of the rings. Consequently, only magnetic excitation exists in Figure 2.9 (a), only electric excitation exists in Figure 2.9(c). Both excitations are observed in Figure 2.9(b) and the structure is not excited in Figure 2.9(d).

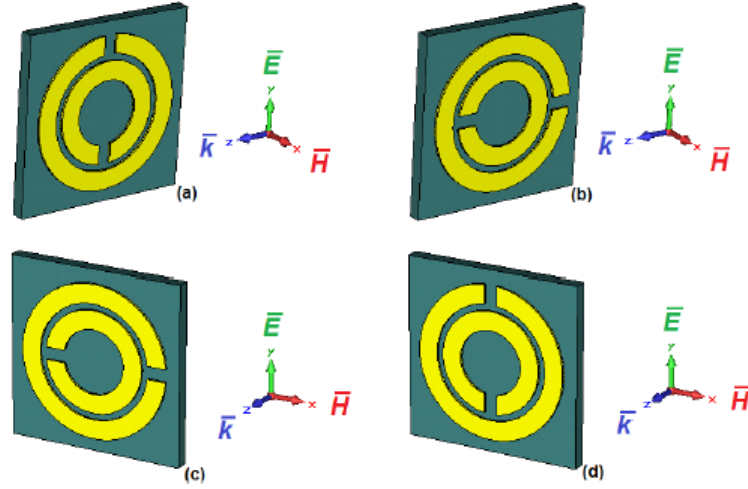


Figure 2.9 Excitation types a) Magnetic excitation b) Electric and magnetic excitation c) Electric excitation d) No excitation (Ekmekçi, 2010).

It can be said that the excitation types, shapes and sizes of SRRs are so important in order to obtain negative values of ϵ and μ in specified frequency band. During the last decade, a lot of types of different resonators are proposed and metamaterial structures having split ring resonators are varied (Ekmekçi, & Turhan-Sayan, 2009).

2.3.2 Dielectric Resonators Based Metamaterials

Dielectric resonators (DRs), are materials which have a large dielectric constant ranging from 30 to 100 with temperature stability. They are compact devices with high Q factor and low loss since there exists no metal in the structure. The size reduction due to the high dielectric constant (ϵ_r) is the main reason for using a dielectric resonator in microwave applications requiring high Q resonant structures such as oscillators, amplifiers, and filters.

Dielectric resonators can be mounted in waveguide and they act as filters (Plourde, & Ren, 1981). Various shapes of DRs are given in Figure 2.10.

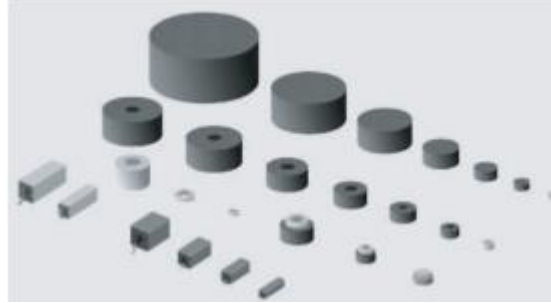


Figure 2.10 Some dielectric resonators (Wang et al., 2009).

It is possible to obtain left-handed material using dielectric resonators. DRs based metamaterial structures have been focused by many researchers. Cubic or cylindrical dielectric resonator based metamaterials are proposed at different frequency regime in the literature (Wang et al., 2009). The negative values of effective permittivity and permeability are obtained in the proper resonance mode. Figure 2.11 is an example of DRs based metamaterial structures (Wang et al., 2009). The negative permittivity and permeability extraction of this geometry will be explained in detail.

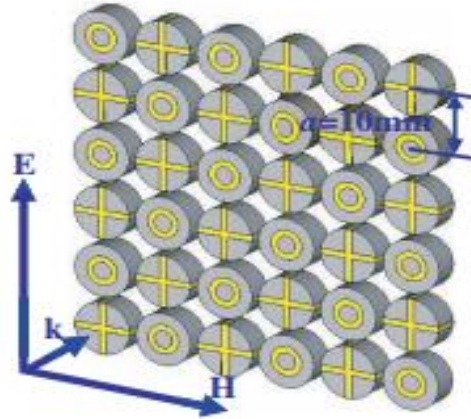


Figure 2.11 Array of dielectric resonators having negative permeability and negative permittivity unit cells (Wang et al., 2009).

Figure 2.12 shows another example of metamaterial employing DRs forming parallel plate (Ueda, Lai, & Itoh, n. d). In this structure $TE_{01\delta}$ mode for DRs is used to obtain negative permeability. DRs are placed in cutoff background, and this

provides negative permittivity. Experimental results related to this example can be found in (Ueda, Lai, & Itoh, n. d).

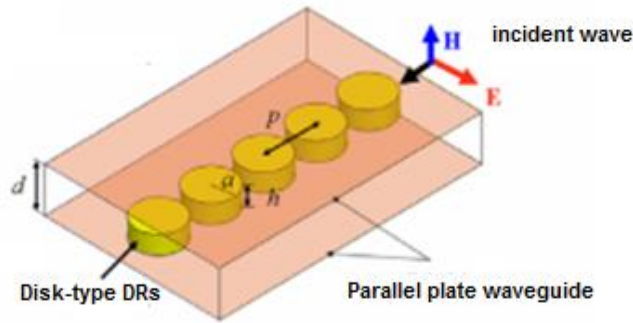


Figure 2.12 Dielectric resonator metamaterials in parallel plate waveguide (Ueda et al., n. d).

2.4 Applications of Metamaterials

Applications of metamaterials have increased enormously in the last decades, since they have got a lot of advantages such as compact size in different application areas. Some of the typical application areas are summarized below..

2.4.1 Frequency Selective Surface Based Metamaterial

Frequency selective surfaces (FSSs) have been produced to control the frequency spectrum of the signal for eliminating noise and undesired interference. Besides, FSSs are commonly used in the design of radomes of the antennas and to reduce radar cross section of the targets. The characteristics of FSSs are described by their geometry producing a periodic structure. Traditional FSSs should have the elements with the optimum lengths of about $\lambda/2$ at the desired frequency to give the best performance (minimum reflection or maximum transmission); however, when they are used in a periodic structure, the total area of FSS can increase significantly. On the other hand, by using metamaterials, this length as well as the periodicity of the array in FSS can be reduced to $\lambda/10$ or below. For this purpose, several studies investigate metamaterial structures that exhibit frequency selective properties (Bayatpur, 2009; Oraizi & Afsahi, 2009) in literature. In Figure 2.13, an example of metamaterial based FSS is depicted such that the structure has the dimensions of 1λ by 1λ (Bayatpur, 2009). If a classical FSS is used for the same purpose, the

dimensions will be about 5λ by 5λ resulting in 25 times larger total area as compared to that of metamaterial based FSS. Therefore, the desired performance at the selected frequency band can be accomplished with much compact sizes.

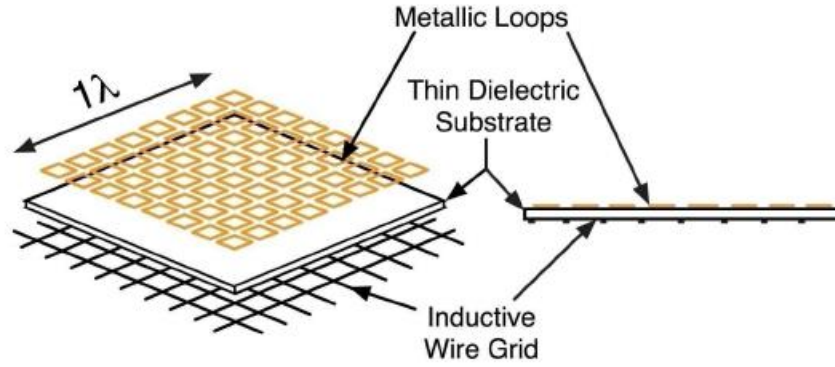


Figure 2.13 The loop wire metamaterial based FSS (Bayatpur, 2009).

2.4.2 Metamaterial Antennas

Metamaterial-based antennas exhibiting negative permittivity or/and negative permeability form an important class of antennas. Metaterials, which have negative permeability or permittivity, may provide electrically small antenna size. The important features of metamaterial antennas are high directivity, tunable operational frequency, control of the direction of antennas. Besides, metamaterial-based antenna can enhance efficiency and bandwidth performance (Chen, & Alu, 2010; Majedi, & Attari, 2013; Kim, & Varadan, 2010; Sahu et al., 2013; Dong, & Itoh, 2012; Xiong, Hong, Tan, & Li, 2013).

For example, metamaterial CNC-shaped resonator in Figure 2.14 achieves enhancement of gain and bandwidth in applications at 5.5 GHz and Wimax technology (3.3-3.8 GHz) (Upadhyaya, Kosta, Jyoti, & Palandoken, 2014).

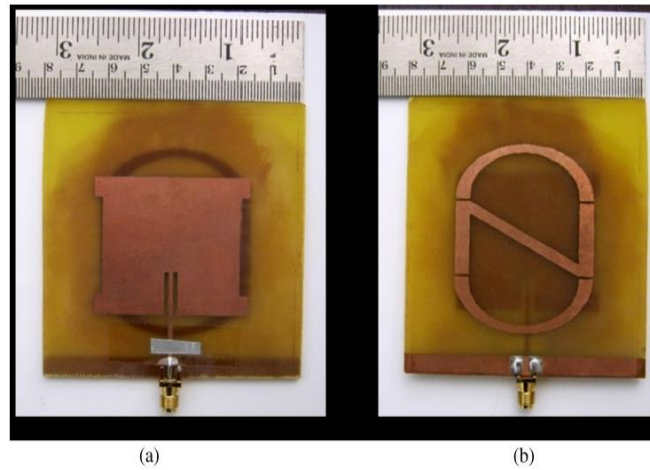


Figure 2.14 An example of metamaterial antenna (Upadhyaya et al., 2014).

Another example of metamaterial based antenna is shown in Figure 2.15. In this study, metamaterial array is used as superstrate to increase directivity of the cylindrical dielectric resonator antenna. Also, the gain and bandwidth of antennas has been increased (Sahu et al., 2013).

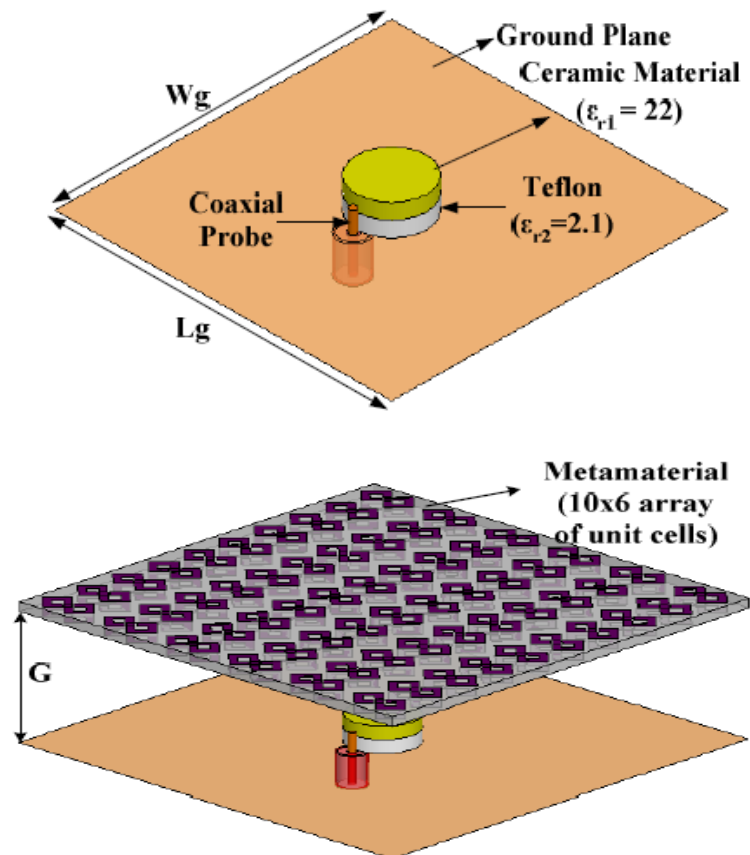


Figure 2.15 An example of metamaterial antenna with dielectric resonator (Sahu et al., 2013).

2.4.3 Metamaterial Power Divider and Coupler

In microwave application, power divider and coupler are important devices. In recent years, multiband or wideband power dividers and couplers are required for multiband/wideband mobile systems. A traditional power divider usually operates within narrow and single band, so it may not be suitable for these mobile systems. In literature, power dividers based on the metamaterial are proposed to achieve multiband or wideband operation. For example, a power divider based on the ring resonator is shown in Figure 2.16 (Jiang, Xu, & Lin, 2013).

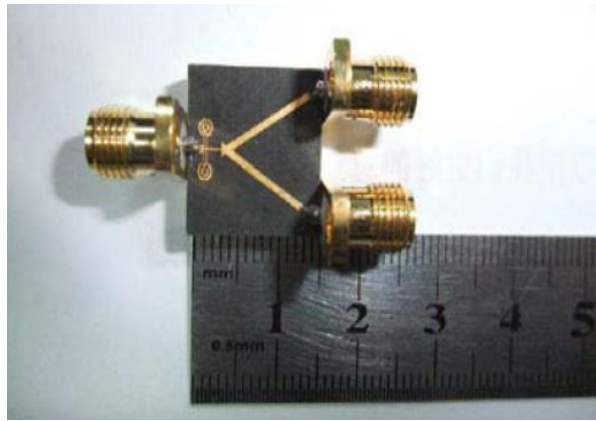


Figure 2.16 A metamaterial based power divider (Jiang et al., 2013).

In the structure in Figure 2.16, two-turns ring resonators are inserted into the input port (left port in Figure 2.16) of the microstrip divider. With the addition of these resonators, a satisfactory impedance transformation to the input port is realized within a wider bandwidth. This divider provides higher than 15 dB return loss for the frequency band of about 4 GHz-6.7 GHz by dividing the power to the output ports almost equally. It is very hard to acquire similar performance with the classical power divider, and this kind of wide bandwidth can be only possible by putting a very bulky and large-size impedance transformer to the input port of the divider. However, the usage of the metamaterial in this divider provides almost 50 percent reduction in the size of the transformer with respect to the divider without metamaterial, so the size of the total structure is significantly decreased.

Similarly, metamaterial-based directional couplers are proposed in literature that one of example is depicted in Figure 2.17 along with a traditional direction coupler (Eleftheriades, 2004).

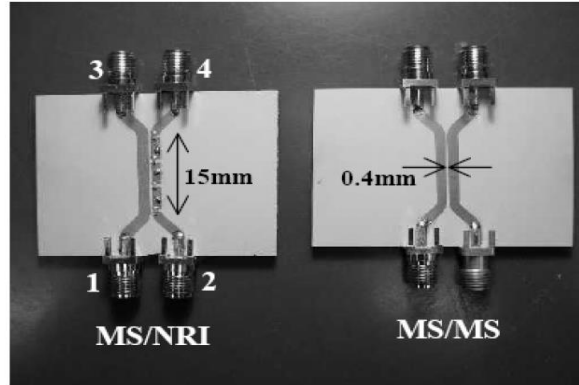


Figure 2.17 Metamaterial based (left) and traditional (right) microstrip directional coupler (Eleftheriades, 2004).

In the study of (Eleftheriades, 2004), the performances of two microstrip directional couplers having exactly same dimensions are compared. The coupler on the right side of Figure 2.17 contains two identical microstrip (MS) lines between port 1 and 3, and port 2 and 4. On the other hand, while the left coupler has MS line between port 1 and 3, a metamaterial based negative-refractive index (NRI) line is implemented between port 2 and 4. This NRI line is realized with periodic unit cells containing shunt inductor and series capacitor. This study reveals that the usage of metamaterial in the microstrip directional coupler results in better coupling and isolation performances by giving higher coupling and isolation values.

2.4.4 Metamaterial Clocking Devices

Cloaking was investigated in 1990s, and it was accomplished that full cloaking could not be possible for all directions of incidence (Wolf, & Habashy, 2007). After that, metamaterial cloaking has made the concept of invisibility of an object revive beginning from 2007. It basically depends on the process of shielding object by controlling propagation of the light, which is described in Figure 2.18 (Pendry, Schurig, & Smith, 2006; Ung, 2009).

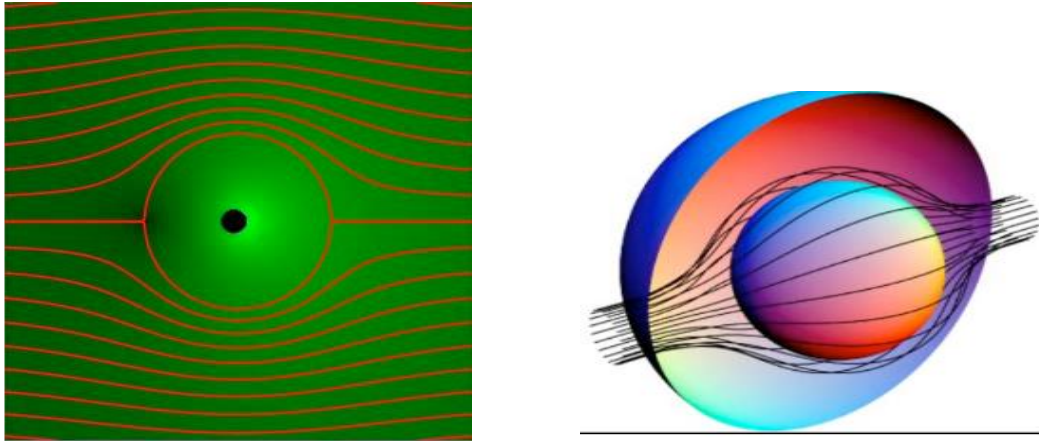


Figure 2.18 Invisible objects (Pendry et al., 2006; Ung, 2009).

For a metamaterial object, the incident light coming from back side of the object creeps around the object and propagates towards the front side of the object. Therefore, an observer (a human) on the front side of the object only sees the incident light coming from back side of the object. Therefore, the object physically exist; however, incident light coming from back side dominates the light reflected from the object, and it makes the object optically invisible. This mechanism can not be possible for ordinary objects due to the fact that the light coming from backside of the ordinary objects can not creep around these objects and go towards to the front side.

2.4.5 Superlens

The imaging resolution limited by diffraction in traditional lenses can be improved by superlens which use metamaterials. In the study of (Pendry, 2000), a superlens is realized, which compensates wave decay and provide better resolution of the image.

In Figure 2.19, the working principle of the superlens is described. A metamaterial medium with negative refractive index bends the incident wave to a negative angle. If the medium was right handed, the wave should diverge from a

point, but due to the negative refractive index, wave here converges to a point (Pendry, 2007).

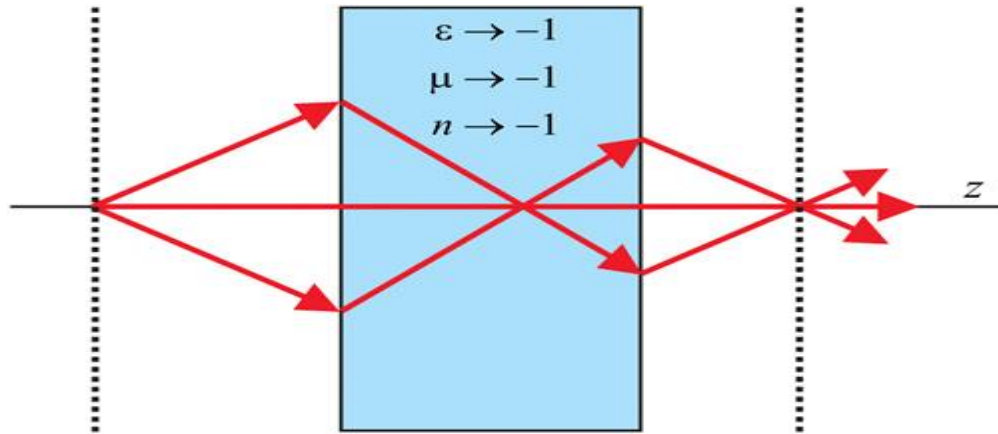


Figure 2.19 Refraction of wave in the metamaterial medium (Pendry, 2007).

CHAPTER THREE

DIELECTRIC RESONATOR BASED METAMATERIAL STRUCTURE

The dielectric resonators are very popular due to their low-loss and high-Q characteristics (Pozar, 2012). They are an alternative to split-ring resonator (SRR) structures, and frequently used in metamaterial applications such as waveguide miniaturization and invisibility (Ueda et al., 2007; Semochkina, Werner, & Pantano, 2010). Similar to SRR structures, the effective medium theory depending on the parameters of effective permittivity and permeability is used in order to analyze the characteristics of metamaterial structures with dielectric resonators. However, in the most of dielectric resonator based metamaterial studies, these parameters are extracted for the cases with the illumination of TEM waves such as free-space or parallel-plate waveguide. Although metamaterial structures based on dielectric resonators contained in a waveguide are presented with their scattering parameters in the literature (Ueda et al., 2010; Chen, Wang, & Semochkina, 2011) previously, to the best of our knowledge, the effective permittivity and permeability values (therefore, the characteristics of being a metamaterial) for the dielectric resonators within a rectangular waveguide supporting non-TEM waves are not presented.

This work presents the extraction of effective permittivity and permeability values for a closely spaced two-element dielectric resonator array where elements are placed in the propagation axis of a standard WR90 rectangular waveguide. For this purpose, the scattering parameters (S_{11} and S_{21}) are first obtained with the simulations, and the results are supported with the measurements. Then, the effective values are obtained by using de-embedding and retrieval processes (Weir, 1974), and the frequencies, which show DNG (both negative permeability and permittivity) characteristics, are observed.

In this respect, Section 3.1 explains the de-embedding process used in the applications. Section 3.2 gives the details of the parameter extraction (retrieval) technique, and Section 3.3 describes the applications and results for both waveguide and free space structures.

3.1 De-embedding Processes

De-embedding is a process which shifts the references planes from measured ones to desired ones. In our applications, the main aim of the de-embedding process is to remove phase shift in the air sections given in Figure 3.1.

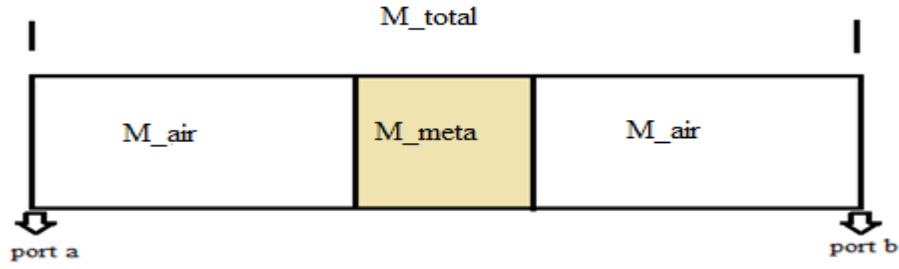


Figure 3.1 The schematic for de-embedding process.

In this figure, M_{meta} is the metamaterial medium, M_{air} is the air section and M_{total} is the total structure.

Initially, S (scattering) parameters are obtained by the measurement or simulations at the reference planes between port a and port b. Then, by using S parameter to T (chain scattering) parameter conversions (Ludwig, & Bretchko, 2000), the elements of the T matrix of the total structure are obtained by the below equations.

$$T_{11} = \frac{1}{S_{21}} \quad (3.1)$$

$$T_{12} = -\frac{S_{22}}{S_{21}} \quad (3.2)$$

$$T_{21} = \frac{S_{11}}{S_{21}} \quad (3.3)$$

$$T_{22} = \frac{-(S_{11}S_{22} - S_{12}S_{21})}{S_{21}} = \frac{-\Delta S}{S_{21}} \quad (3.4)$$

According to the network property of T parameters (Ludwig, & Bretchko, 2000), T matrix of the total structure can be expressed as the cascade of three (air, meta, air) sections:

$$[T_{total}] = [T_{air}][T_{meta}][T_{air}] \quad (3.5)$$

where T_{air} is the T matrix of the air sections, and T_{meta} is the T matrix of the metamaterial medium.

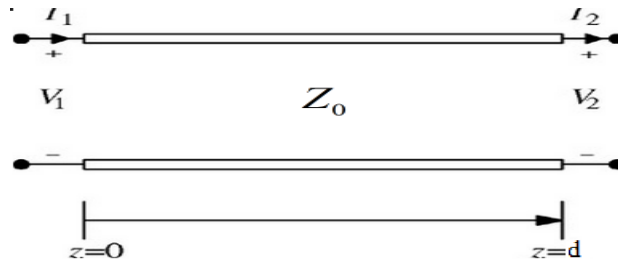


Figure 3.2 A two-port transmission line

Here, in order to obtain T parameter of the air sections, ABCD parameters of the air section are used. The ABCD parameters in terms of the terminal voltages and currents of the guided structure in Figure 3.2 are given in equations as below;

$$\begin{bmatrix} V_1 \\ I_1 \end{bmatrix} = \begin{bmatrix} A & B \\ C & D \end{bmatrix} \begin{bmatrix} V_2 \\ I_2 \end{bmatrix} \quad (3.6)$$

$$A = \cos \beta l \quad (3.7)$$

$$B = jZ_0 \sin \beta l \quad (3.8)$$

$$C = \frac{j \sin \beta l}{Z_0} \quad (3.9)$$

$$D = \cos \beta l \quad (3.10)$$

where Z_0 is the wave impedance of the structure in air and β is the phase constant.

ABCD parameters of air medium are then converted to S parameters with the following equations

$$S_{11} = \frac{A + B/Z_0 - CZ_0 - D}{A + B/Z_0 + CZ_0 + D} \quad (3.11)$$

$$S_{12} = \frac{2(AD - BC)}{A + B/Z_0 + CZ_0 + D} \quad (3.12)$$

$$S_{21} = \frac{2}{A + B/Z_0 + CZ_0 + D} \quad (3.13)$$

$$S_{22} = \frac{-A + B/Z_0 - CZ_0 + D}{A + B/Z_0 + CZ_0 + D} \quad (3.14)$$

After that, T parameters of the air are obtained by using conversion given in the equations (3.1-3.4).

T_{meta} matrix can be obtained by using the equation given below;

$$[T_{meta}] = [T_{air}]^{-1} [T_{total}] [T_{air}]^{-1} \quad (3.15)$$

Finally, S parameters of the metamaterial structure are obtained by using the conversion formulas from T to S parameters as (Ludwig, & Bretchko, 2000)

$$S_{11} = \frac{T_{21}}{T_{11}} \quad (3.16)$$

$$S_{12} = \frac{T_{11}T_{22} - T_{21}T_{12}}{T_{11}} \quad (3.17)$$

$$S_{21} = \frac{1}{T_{11}} \quad (3.18)$$

$$S_{22} = -\frac{T_{12}}{T_{11}} \quad (3.19)$$

3.2 Retrieval Technique

In this section, the retrieval technique for the extraction of the parameters in waveguide and free-space structures will be explained in detail.

Firstly, for waveguide case, the S_{11} and S_{21} parameters of the structure, which has two dielectric resonators in waveguide, are used to obtain the medium parameters, complex ε and μ of the structure. For the required extraction process, the procedure of retrieval method reported in (Ghodgaonkar et al., 1990) is followed in this study.

The S_{11} and S_{21} parameters can be expressed as:

$$S_{11} = \frac{\Gamma(1-\tau^2)}{1-\Gamma^2\tau^2} \quad (3.20)$$

$$S_{21} = \frac{\tau(1-\Gamma^2)}{1-\Gamma^2\tau^2} \quad (3.21)$$

where Γ is the reflection coefficient at the interface between air and metamaterial section, τ is the propagation coefficient within the metamaterial medium.

Using (3.20) and (3.21), the reflection coefficient Γ and propagation coefficient can be expressed as:

$$\Gamma = K \pm \sqrt{K^2 - 1} \quad (3.22)$$

where

$$K = \frac{S_{11}^2 - S_{21}^2 + 1}{2S_{11}} \quad (3.23)$$

$$\tau = \frac{S_{11}^2 - S_{21}^2 + \Gamma}{1 - (S_{11} + S_{21})\Gamma} \quad (3.24)$$

In equation (3.22), Γ should be properly chosen to give that $|\Gamma| < 1$.

The complex permittivity and permeability can be expressed in terms of τ and Γ by using the following equations:

$$\frac{1}{\Lambda^2} = \left(\frac{\epsilon_r \mu_r}{\lambda_0^2} - \frac{1}{\lambda_c^2} \right) = - \left[\frac{1}{2\pi l} \ln \left(\frac{1}{\tau} \right) \right]^2 \quad (3.25)$$

$$\mu_r = \frac{1 + \Gamma}{\Lambda(1 - \Gamma) \sqrt{\frac{1}{\lambda_0^2} - \frac{1}{\lambda_c^2}}} \quad (3.26)$$

$$\epsilon_r = \frac{\left(\frac{1}{\Lambda^2} + \frac{1}{\lambda_c^2} \right)}{\mu_r} \lambda_0^2 \quad (3.27)$$

where l is the length of the metamaterial structure, λ_0 is free-space wavelength and λ_c is cut-off wavelength, which is equal to $2a$ for dominant TE₁₀ mode of the rectangular waveguide.

For free-space case, which supports TEM mode, λ_c in equation (3.25) become infinity, and ϵ_r and μ_r can be again found from equations (3.26 and 3.27).

Alternatively; the reflection coefficient Γ and propagation coefficient τ seen in equations (3.22) and (3.24) can be expressed as

$$\Gamma = \frac{(Z_{sn} - 1)}{(Z_{sn} + 1)} \quad (3.28)$$

where Z_{sn} is the normalized characteristic impedance with respect to the wave impedance of free-space and is related to $\mu_r^* = \mu_r' - j \mu_r''$ and $\varepsilon_r^* = \varepsilon_r' - j \varepsilon_r''$ as shown below:

$$Z_{sn} = \sqrt{\frac{\mu_r^*}{\varepsilon_r^*}} \quad (3.29)$$

From (3.28) and (3.29)

$$\sqrt{\frac{\mu_r^*}{\varepsilon_r^*}} = \left(\frac{1+\Gamma}{1-\Gamma} \right) \quad (3.30)$$

Also we know that the propagation factor is defined as

$$\tau = e^{-\gamma l} = e^{-(\alpha + j\beta)l} \quad (3.31)$$

where γ is propagation constant, α is attenuation constant, β is phase constant.

Using equation (3.31), the propagation constant can be obtained as

$$\gamma = \frac{\left[\ln \left(\frac{1}{\tau} \right) \right]}{d} \quad (3.32)$$

If τ is defined as

$$\tau = |\tau| e^{j\phi} \quad (3.33)$$

then, γ is expressed as

$$\gamma = \frac{\left[\ln \left(\frac{1}{|\tau|} \right) \right]}{d} + j \left[\frac{2\pi n - \phi}{d} \right] \quad (3.34)$$

where $n = 0, \pm 1, \pm 2, \dots$.

These parameters are related to the permittivity and the permeability as follows:

$$\gamma = \gamma_0 \sqrt{\epsilon_r^* \mu_r^*} \quad (3.35)$$

where $\gamma_0 = (j2\pi / \lambda_0)$ describes the propagation constant of free-space.

From equation (3.30) and (3.35), the complex relative permittivity and the complex relative permeability are expressed as;

$$\epsilon_r^* = \frac{\gamma}{\gamma_0} \left(\frac{1-\Gamma}{1+\Gamma} \right) \quad (3.36)$$

$$\mu_r^* = \frac{\gamma}{\gamma_0} \left(\frac{1+\Gamma}{1-\Gamma} \right) \quad (3.37)$$

According to the signs of the complex relative permittivity and the complex relative permeability, the structure can be said to be either right-handed material or left-handed material.

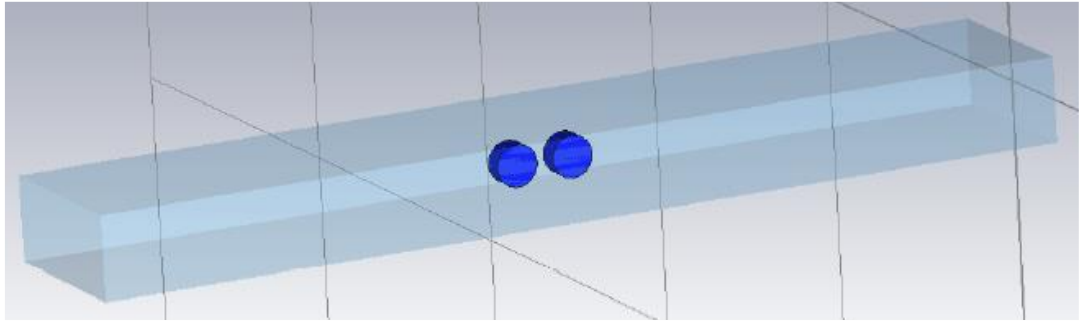
These equations are coded in Matlab, and corresponding codes can be found in Appendix 1.

3.3 The Structure (In Rectangular Waveguide and Parallel Plate Waveguide)

The structure in this work includes two identical cylindrical dielectric resonators as shown in Figure 3.3 (a). The height and the diameter of the resonators are given as 2.53 and 5 mm, respectively. The dielectric constant is measured as about $\epsilon_r = 38$, and this value is also used in the simulations. The (edge-to-edge) distance between

the resonators is selected as $d = 2$ mm. This value is deliberately chosen as being much smaller than the diameter (the dimension in the direction of propagation) in order to provide strong mutual coupling effects between the resonators.

The dielectric resonators are placed along the propagation axis in a standard WR90 rectangular waveguide with the dimensions of 22.86 mm by 10.16 mm. For this purpose, the resonators are embedded in a foam structure ($\epsilon_r = 1.025$) as shown in Figure 3.3(b), and the foam structure with resonators is inserted into the waveguide.



(a)



(b)

Figure 3.3 (a) Simulation view and (b) photograph of structure.

The operating frequency is selected as 8-14 GHz at which dominant TE_{10} mode of the rectangular waveguide propagates. The simulations are carried out with CST Microwave Studio 2014, and the measurements are realized by the experimental setup given in Figure 3.4.

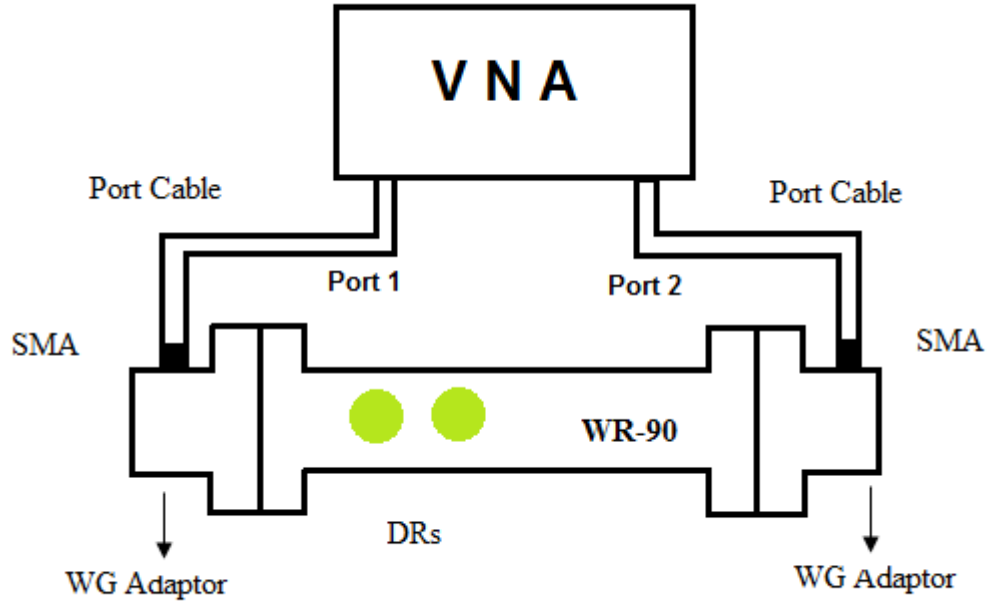
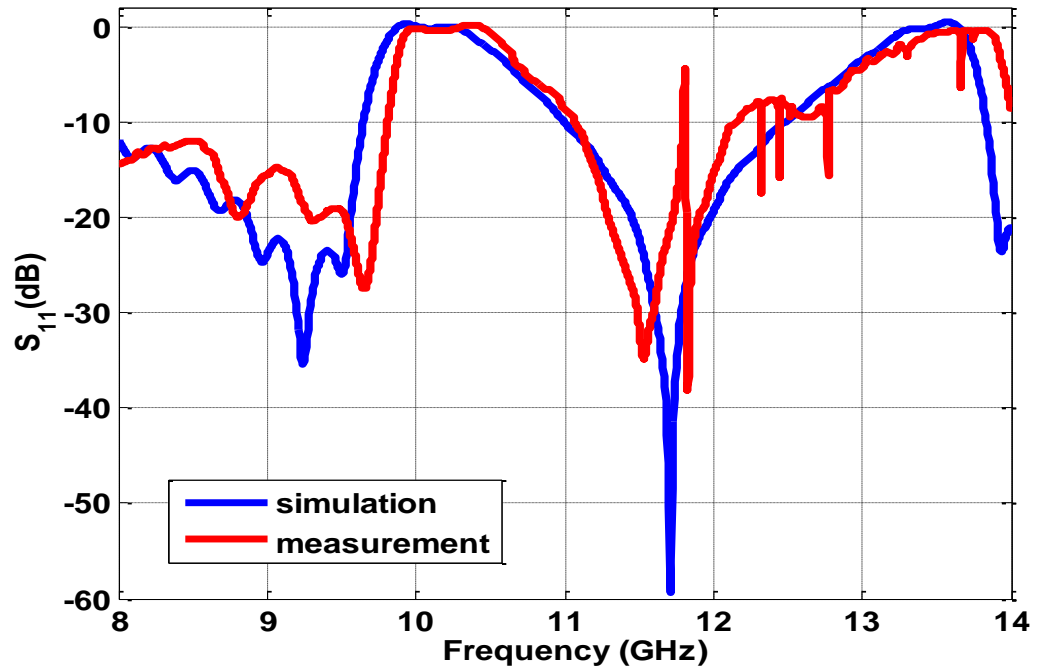


Figure 3.4 The experimental setup for two DRs within the waveguide structure.

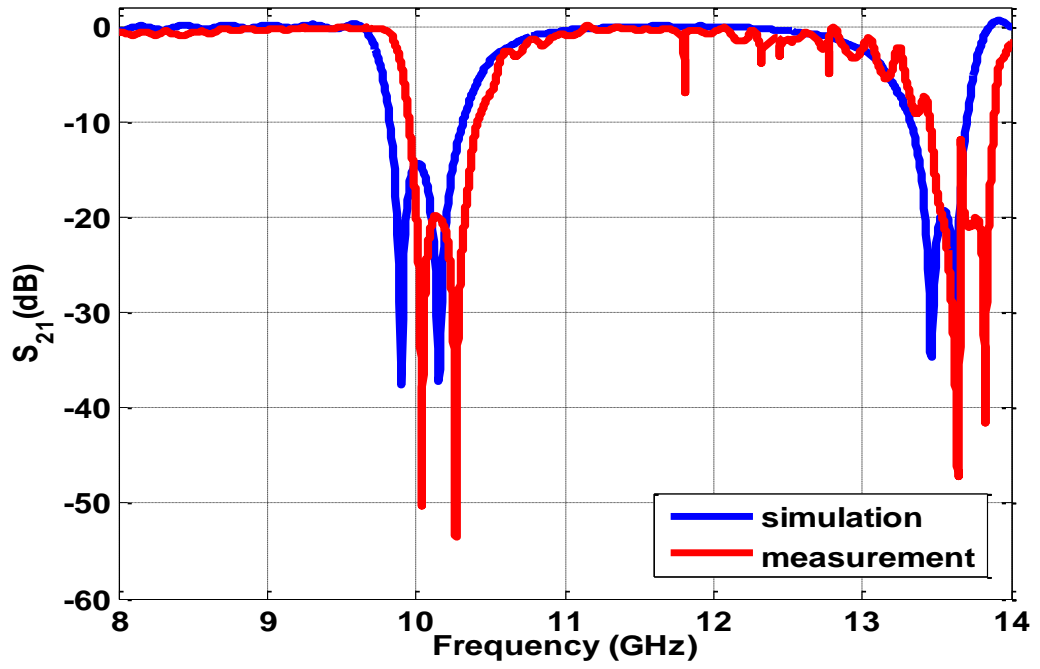
The vector network analyzer (VNA) used in the setup is Anritsu MS4642A in Antenna and Microwave Laboratory of Dokuz Eylül University. The setup is calibrated from SMA connector of the port cable by performing 12-term SOLT (short-open-line-thru) calibration technique. A waveguide (WG) adaptor is attached to each port of the VNA. The WR90 structure with two DRs, which is given in Figure 3.3(b), is inserted between these WG adaptors. By using the *transmission and reflection modes* of the VNA, S_{21} and S_{11} parameters are measured, respectively.

3.3.1 The Results of Waveguide Structure

By realizing the necessary simulations and the measurements for the structure given Figure 3.3, the corresponding scattering parameter (S_{11} and S_{21}) values are obtained. The simulated and measured magnitudes of the responses in dB are depicted in Figure 3.5. The small shifts between the resonance frequencies of the measurement and the simulation do not exceed 1%, and are due to small errors in mechanical arrangement of the resonators within waveguide.



(a)



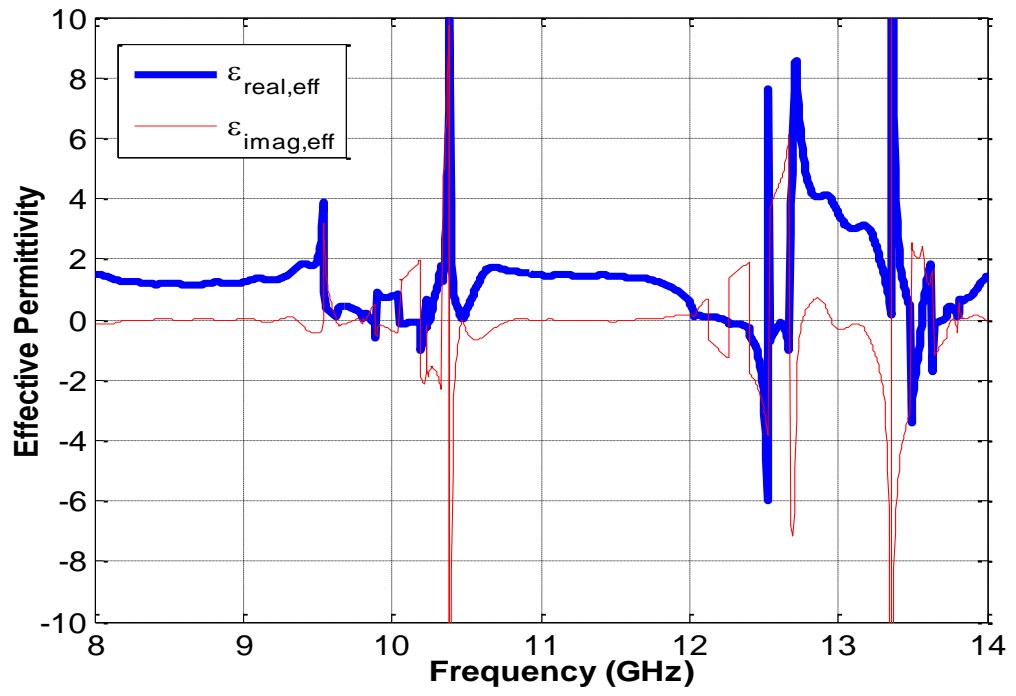
(b)

Figure 3.5 (a) S_{11} (dB) and (b) S_{21} (dB) of the two dielectric resonator array within the rectangular waveguide structure.

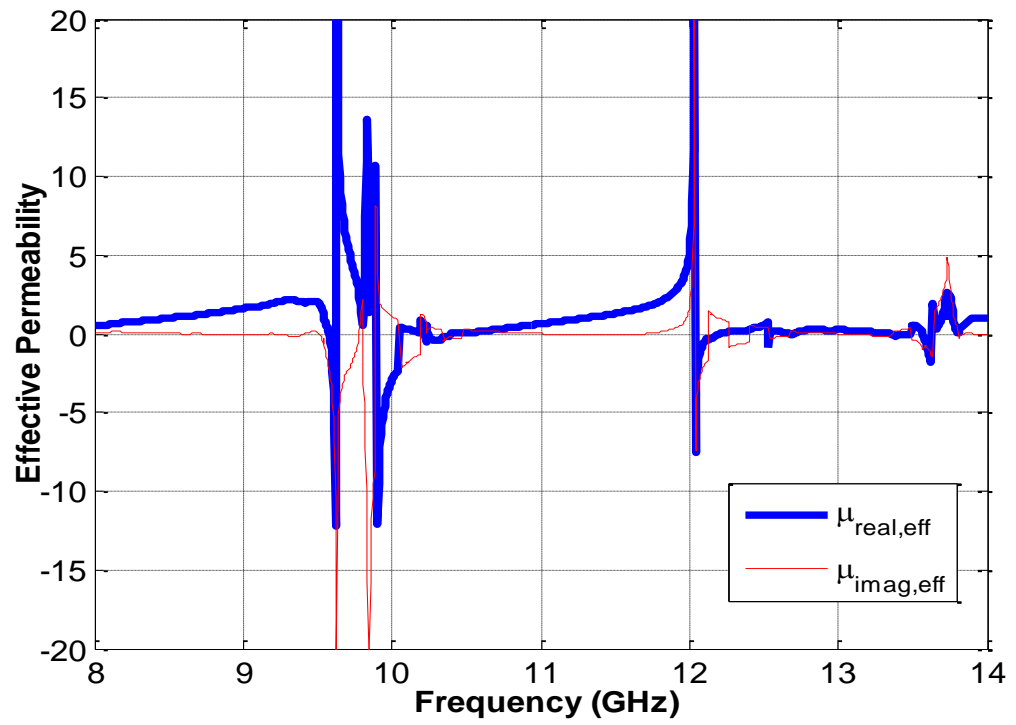
When the response in Figure 3.5 (b) is observed, the double resonance effect, which is a crucial indicator about the characteristics of double negative material, can be seen at the frequencies around 10 GHz (9.9 GHz and 10.15 GHz) and 13.5 GHz (13.47 GHz and 13.62 GHz).

The scattering parameters obtained by the simulations and the measurements are processed to extract the effective permittivity and permeability of the structure via de-embedding and retrieval techniques. The corresponding results for the complex permittivity and permeability are given in Figure 3.6 for the scattering parameters obtained from the simulations since they are consistent with the measured ones. When the effective values in Figure 3.6 are examined, the permittivity has negative values at 9.89, 10.2, 12.52, 13.49 and 13.64 GHz; whereas, the permeability is negative at 9.62, 9.9, 10.23, 12.04, 13.43 and 13.62 GHz.

It is shown that for the frequencies at which both the permittivity and the permeability are negative, the structure possesses double negative (DNG) characteristics at about 9.9, 10.2, 13.45 and 13.65 GHz, which are also consistent with the resonance frequencies in Figure 3.5 (b). Therefore, the metamaterial behavior of the structure is demonstrated that the structure can be used and designed for different metamaterial applications.



(a)



(b)

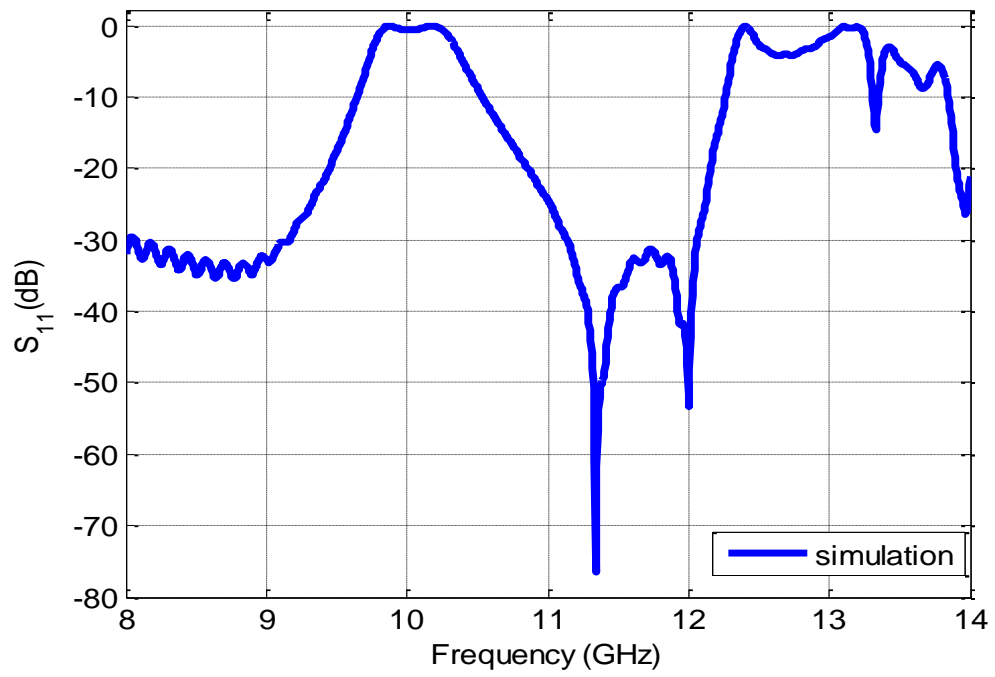
Figure 3.6 (a) Effective permittivity and (b) permeability of the structure for the rectangular waveguide.

3.3.2 Results of Parallel-Plate Waveguide Structure

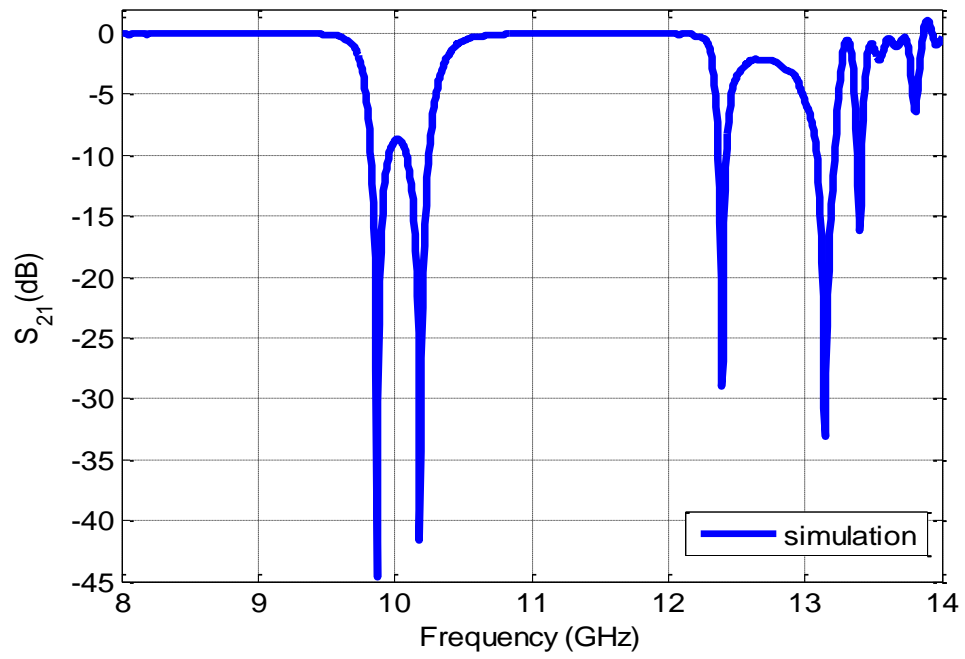
In order to observe the behaviour of the metamaterial structure when the mode type is changed, a different structure rather than rectangular waveguide is investigated. This structure consists of parallel plate waveguide which supports TEM mode.

TEM mode is realized in CST Microwave Studio by just changing the boundary conditions on side walls of the waveguide from perfect electric to perfect magnetic. Perfect electric boundary means that the tangential components of the electric field on the surface is zero, perfect magnetic boundary means that the tangential components of the magnetic field on the surface is zero.

The scattering parameters values of the consist of two DRs structure realized with simulation in parallel-plate waveguide are shown as Figure 3.7. As seen from the figure, there is double resonance effect about 10 GHz (9.9 GHz and 10.15 GHz), and 13.25 GHz (13.15 GHz and 13.40 GHz). In this manner, these results are consisted with those of waveguide structure. The effective permittivity and the effective permeability coefficients of both structures are obtained by using de-embedding and retrieval processes with resulting scattering parameters. The corresponding results for the complex permittivity and the complex permeability are given Figure 3.8 from the simulations for parallel-plate waveguide structure.

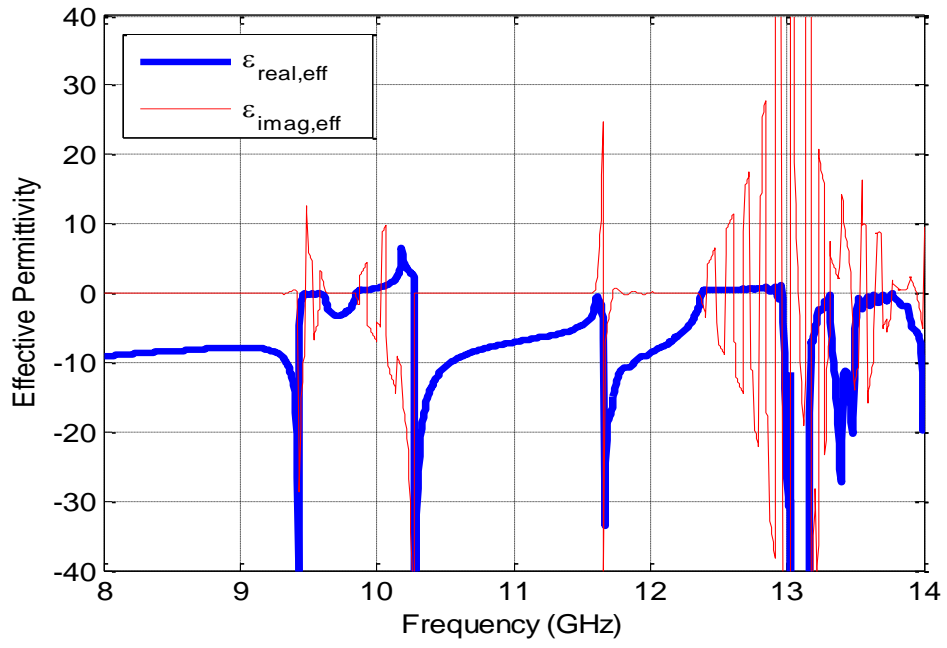


(a)

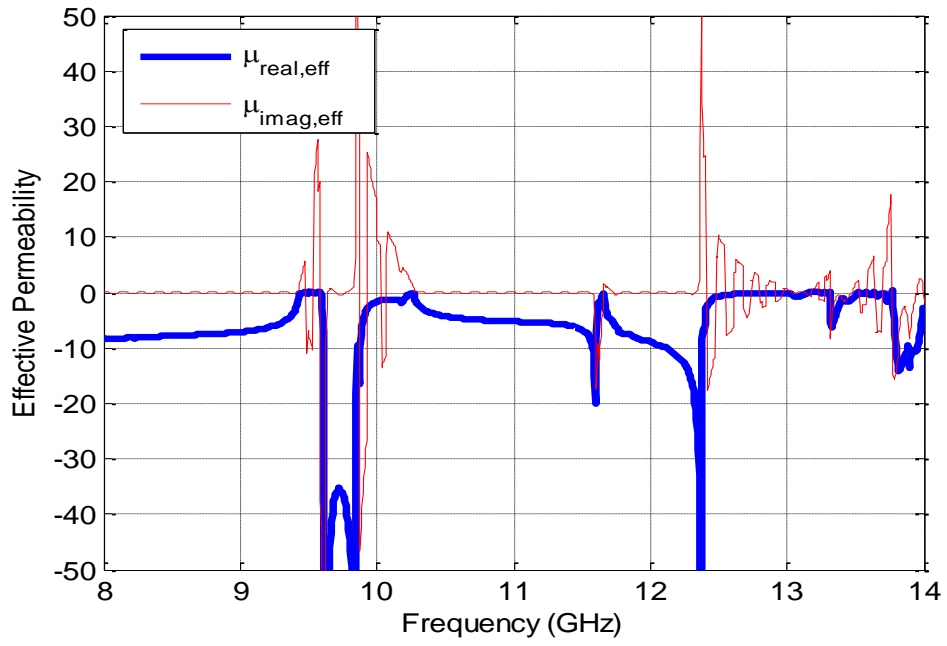


(b)

Figure 3.7 (a) S_{11} (dB) and (b) S_{21} (dB) the two dielectric resonator array in parallel-plate waveguide.



(a)



(b)

Figure 3.8 (a) Effective permittivity and (b) Effective permeability for parallel-plate waveguide.

By considering results of Figure 3.6 and Figure 3.8, the frequencies at which both real and imaginary part of the effective permittivity and permeability are negative at the same time are extracted. The results related to this is given in Table 3.1. According to the results given in Table 3.1, it is shown that for the common frequencies at which both the permittivity and the permeability are negative, the structure based waveguide possesses double negative (DNG) characteristics at about 9.9, 10.2, 13.45 and 13.65 GHz which are also consistent with the double resonance frequencies in Figure 3.6 (b). Similarly, the parallel-plate waveguide structure possesses double negative (DNG) characteristics at about 9.6, 9.9, 11.6, 13.4 and 13.9 GHz and can be said to be consistent with double resonance frequencies in Figure 3.8 (b). The obtained DNG metamaterial characteristic frequencies for both structures are very closed each other. It can be concluded that the sensitivity of the metamaterial structures to the different wave excitation (TEM mode for parallel-plate waveguide; TE₁₀ for rectangular waveguide) is slight.

Table 3.1 Comparison of the negative values of ϵ and μ in rectangular waveguide and parallel plate waveguide.

Rectangular Waveguide		Parallel-Plate Waveguide	
ϵ	μ	ϵ	μ
-	9.62 GHz	9.44 GHz	9.6 GHz
9.89 GHz	9.9 GHz	10.1 GHz	9.9 GHz
10.2 GHz	10.23 GHz	10.27 GHz	-
12.52 GHz	12.04 GHz	11.67 GHz	11.6 GHz
13.49 GHz	13.43 GHz	13.48 GHz	13.38 GHz
13.64 GHz	13.62 GHz	13.9 GHz	13.9 GHz

CHAPTER FOUR

APPLICATION OF DIELECTRIC RESONATOR BASED METAMATERIAL STRUCTURE IN WAVEGUIDE COUPLER

In this chapter, it is aimed to observe the behaviour of the dielectric resonator based metamaterial structure in multihole (Bethe hole) waveguide coupler. The name of the component comes from the study of H. A. Bethe named “Theory of Diffraction by Small Holes” made in 1944 (Bethe, 1944). The coupling and isolation performances of the coupler are desired to be improved by inserting the metamaterial structure in the near of isolation port of the waveguide coupler.

4.1 Theory of Multihole Waveguide Coupler

Couplers are passive microwave components designed for power division. The difference between power divider and coupler is that coupler generates phase shift between output signals. The main aim of coupler is to take a small portion (usually between %1 and %25) of the signal, so that the incident power on a transmission line can be observed without too much loss. Various types of couplers are available in microwave applications such as the coupled line directional couplers, waveguide magic-T, ring hybrid.

One of the ways of coupling is to open small holes in the wall shared by two parallel rectangular waveguides. Bethe hole coupler, which is given in Figure 4.1, is a typical example of these kinds of coupling (Pozar, 2012).

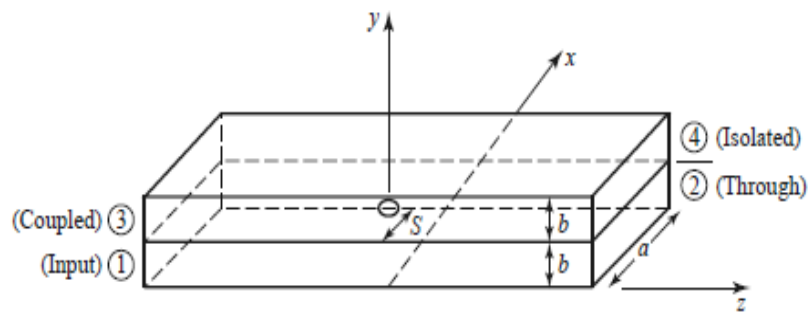


Figure 4.1 A typical Bethe hole directional coupler (Pozar, 2012).

Several terms such as coupling (C), insertion loss (IL), isolation of a coupler (I), and directivity (D) are used to characterize a coupler.

Using the port references given in Figure 4.1, coupling (C) is defined in terms of coupled power (P_3) and the input power (P_1), that is;

$$C = -20 \log(|S_{31}|) \quad (4.1)$$

The insertion loss between the input and through ports is defined as

$$IL = -20 \log(|S_{21}|) \quad (4.2)$$

The isolation of a coupler how the power ratio input between the input and the isolated port. It is given by

$$I = -20 \log(|S_{41}|) \quad (4.3)$$

The directivity is defined as direct energy only to desired port. It is given by

$$D = -20 \log \left(\frac{|S_{31}|}{|S_{41}|} \right) \quad (4.4)$$

or

$$D = I - C \quad (4.5)$$

Since this coupler is symmetric coupler, its scattering matrix should be ideally in the form of following equation at the center frequency (Pozar, 2012).

$$[S] = \begin{bmatrix} 0 & \alpha & j\beta & 0 \\ \alpha & 0 & 0 & j\beta \\ j\beta & 0 & 0 & \alpha \\ 0 & j\beta & \alpha & 0 \end{bmatrix} \quad (4.6)$$

For a lossless coupler, $|\alpha|^2 + |\beta|^2 = 1$ should hold.

Bethe hole coupler has narrow bandwidth. The bandwidth can be enhanced wider by increasing the numbers of holes. This type of coupler is called as multihole coupler. By arranging the diameter of the hole and the number of the holes, the maximum radiation can be achieved in the coupling port, and the radiation in the isolated port can be cancelled. This mechanism is depicted in Figure 4.2 for a two-hole structure.

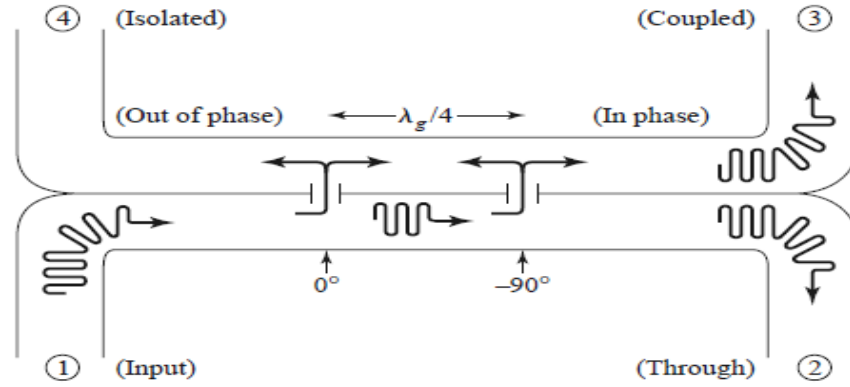


Figure 4.2 Working mechanism of two-hole coupler (Pozar, 2012).

The wave coupled from hole 2 to the isolated port propagates $\lambda_g / 2$ further than the wave coupled from hole 1 to the same port. Therefore, there is a 180° phase shift between the waves coming from hole 1 and hole 2. It causes a cancellation in the isolated port. The path lengths of the waves coupled from hole 1 and hole 2 to the coupled port are the same; so these waves are added in phase.

4.2 Performance Analysis of Coupling and Isolation with Metamaterial Structure

The structure of dielectric resonators used as a metamaterial in waveguide is mentioned in Chapter 3. It is observed that two dielectric resonators cause two double resonances. Besides, as the number of dielectric resonator increases, the bandwidth of the structure increases. In this section, the changes in the performances of coupling and isolation of a waveguide Bethe hole coupler are analyzed when dielectric resonators are placed inside the coupler.

As an example, a four-hole coupler with the hole radii as $r_0= 3.26$ mm, $r_1=4.51$ mm, $r_2= 4.51$ mm and $r_3= 3.26$ mm is designed in a WR90 waveguide to give around 20 dB coupling and below 40 dB isolation for the frequency band of 8-10 GHz. The details of this design can be found in Appendix 2. The center to center distance between the holes is kept as constant value of 12.17 mm, which is quarter of guided wavelength at the center frequency of 9 GHz (Pozar, 2012).

The four-hole in common wall Bethe coupler is drawn as shown in Figure 4.3, and the corresponding simulations are carried out with CST Microwave Studio 2014.

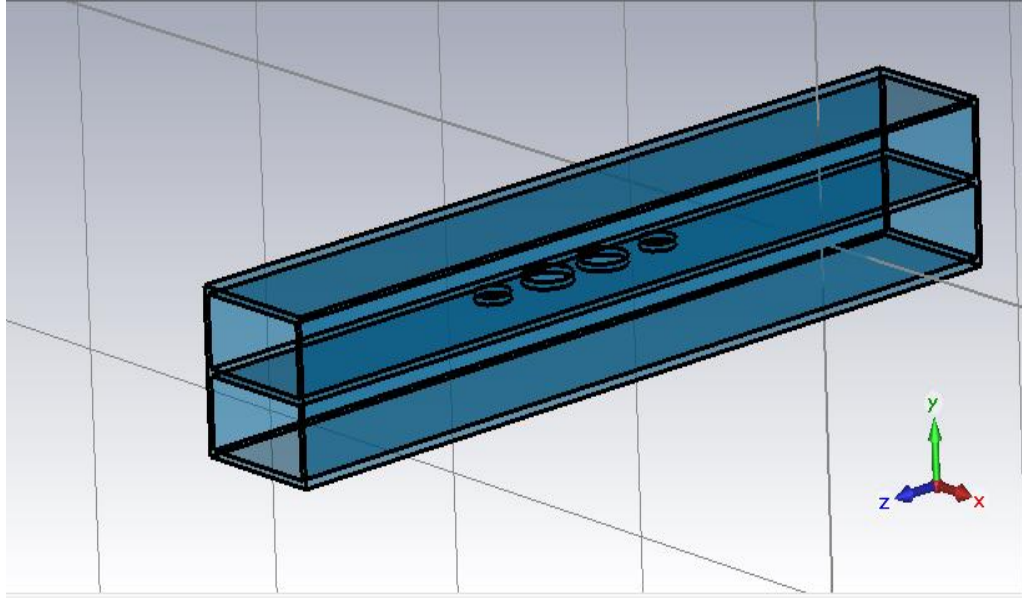


Figure 4.3 Simulation view of four-hole coupler.

The distance from centers of the holes to the edge wall of the waveguide, which is given as s in Figure 4.1, is selected as $s = a/4$ where $a = 22.86$ mm is the width of the rectangular waveguide used in this example. The length of both waveguide is selected as 150 mm.

The simulated coupling (S_{31}) and isolation (S_{41}) responses of the structure are plotted in Figure 4.4. As shown in Figure 4.4, multihole coupler operates at the frequency band of 8-10 GHz (and with the center frequency of 9 GHz) by giving around 20 dB coupling. The coupling changes by almost 1 dB along the band, which

is highly consistent with theoretical results. The isolation, which depends on the cancellation in the isolated port due to two wave components having a phase shift between them, is again found to be above 40 dB at the desired frequency. Although both simulation and theoretical results contain isolation above 40 dB in the given band, the response curves are slightly different to each other. This is due to the fact that the theoretical calculations are done by obeying the small aperture coupling theory. However, the selected aperture diameters are not sufficiently small, which brings a small differences between the results of theory and simulations.

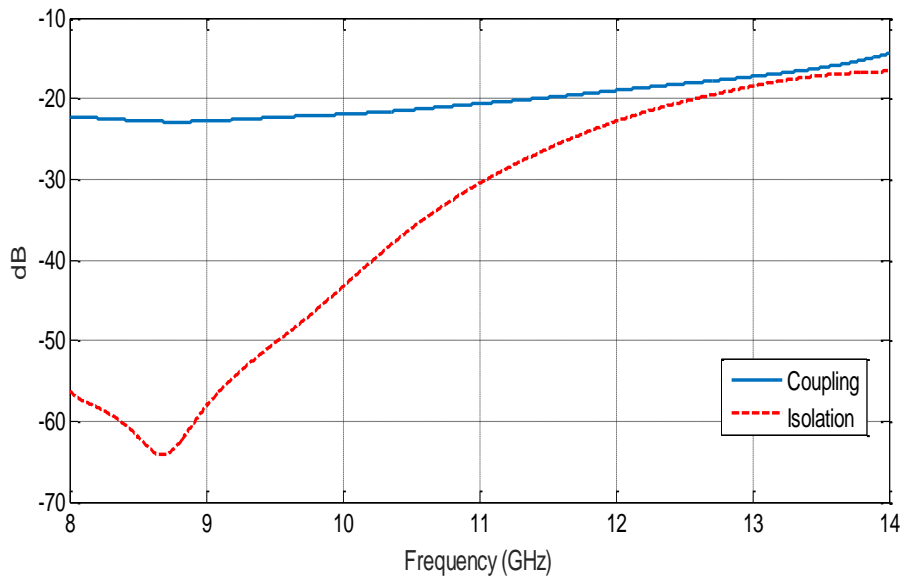


Figure 4.4 Coupling and isolation of multihole coupler without dielectric resonators.

When the results in Figure 4.4 are observed for the overall band (8-14 GHz) of the simulations, which is the same frequency band used in the simulations at Chapter 3, the coupler can be said to be operating at the frequency band of 8-10 GHz. In the overall band, the coupling of the coupler reduces to almost 14 dB, and the isolation drops to around 15 dB. The coupler has the worst performance at the frequency band of 13-14 GHz among the overall band. On the other hand, in Chapter 3 it is shown that two DRs array in waveguide structure behaves as a metamaterial in this band.

By considering this result, an idea has come out that whether this dielectric resonator array inserted into the coupler can have a constructive effect to improve the

coupling and isolation performances of the coupler in the overall band, and to add a new working band at frequency band of 13-14 GHz or not. For this purpose, the array of two dielectric resonators, which is exactly same as the one used in Chapter 3, is placed between isolated port and the holes as shown in Figure 4.5.

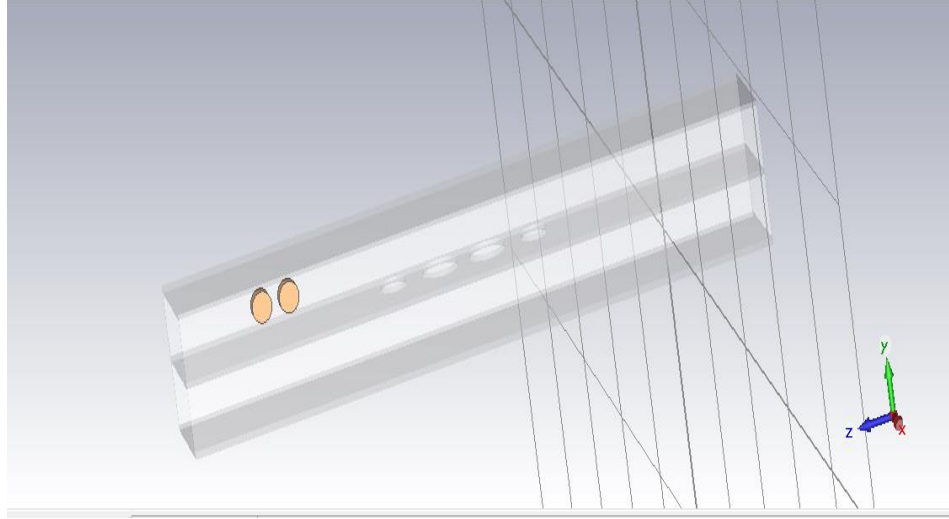


Figure 4.5 Simulation view of four-hole coupler with two dielectric resonators.

The simulations are again realized in CST, and the changes in the performance of the coupling and isolation are analyzed. The coupling (S_{31}) and the isolation (S_{41}) responses of the structure with two dielectric resonators are shown as Figure 4.6.

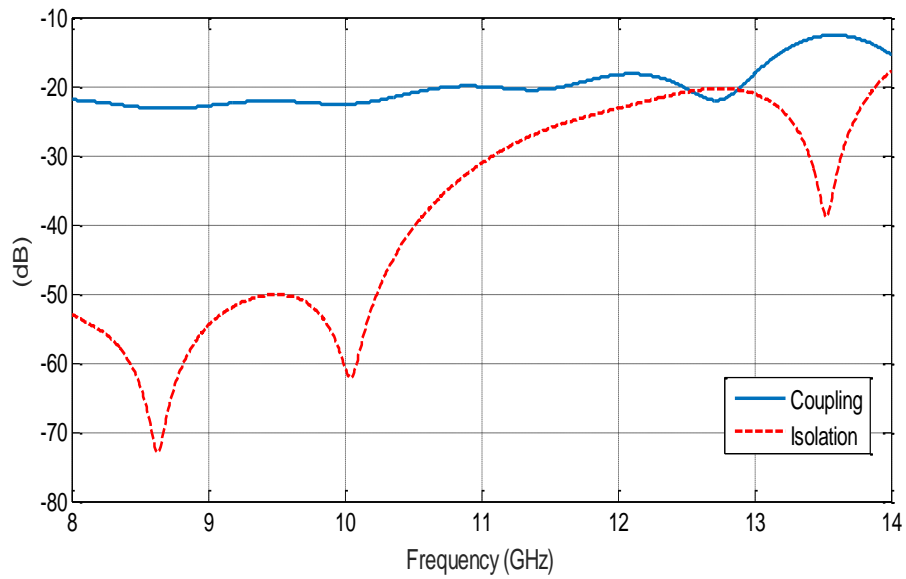


Figure 4.6 The coupling and the isolation of multihole coupler with two dielectric resonators.

According to the results in Figure 4.6, it can be deduced that the isolation is above 20 dB in the overall band, and has minimum 30 dB in the frequency band of about 13.4-13.6 GHz, which is one of the frequency bands where the dielectric resonators have the metamaterial characteristics. Thus, a new operation band (the frequency band of 13.4-13.6 GHz) can be said to be added to the coupler in terms of isolation. However, the coupling performance of the structure with dielectric resonators is not so pleasant such that the coupling value decreases to 12 dB in the overall band, and it unfortunately reaches to these undesired values in the frequency band of 13.4-13.6 GHz at which isolation performance is sufficiently enhanced. Therefore, it can be concluded that this structure (with two dielectric resonators) neither improves the performance of the coupler nor can add a new working band to the coupler.

In order to compare the results of the Bethe hole structure with and without dielectric resonators, the coupling and isolation responses are given in Figure 4.7 and Figure 4.8, respectively. When the results of isolation responses are examined, the S_{41} values are decreased by the structure with dielectric resonators in the overall band even in the original operating frequency band of 8-10 GHz. This is because the dielectric resonator array has also a metamaterial characteristic at around 10 GHz, which creates a reduction in the S_{41} value at this frequency. According to the results in Figure 4.7, the structure with dielectric resonator can be said to have sufficient coupling performance for the frequency of 8-13 GHz at which the coupling is above 18 dB. Actually, when the frequency band of 8-13 GHz is only considered, it can be observed that the structure containing metamaterial highly improves the values of both coupling (with the values above 18 dB) and isolation (with the values above 20 dB) as compared to the one without metamaterial. However, when the frequency band of 13-14 GHz is added to the results, the coupling values decay to 12 dB, which is worse than the case of the structure without metamaterial. Therefore, the performance of the structure with two dielectric resonators, which gives coupling values above 12 dB, is not found to be sufficiently good when the overall band of 8-14 GHz is considered.

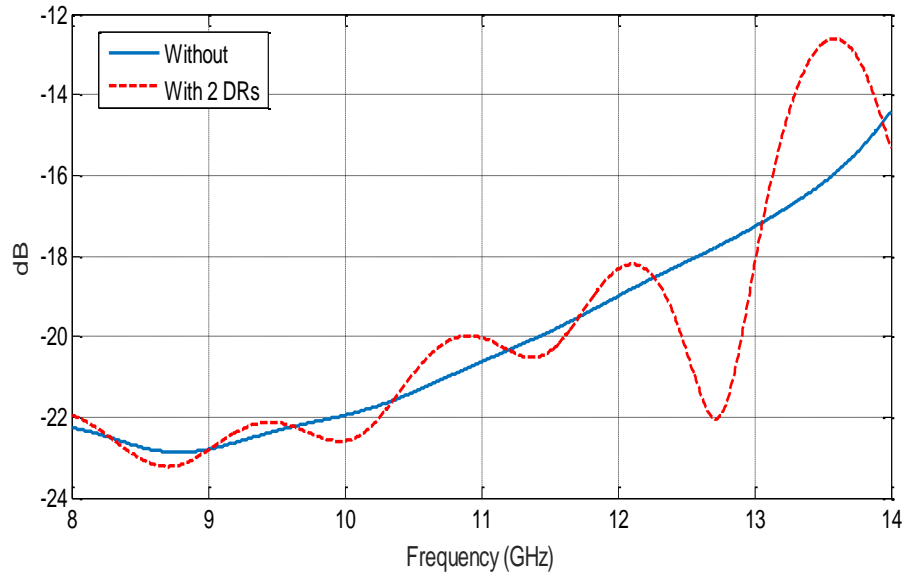


Figure 4.7 Coupling of multihole coupler with and without two dielectric resonators.

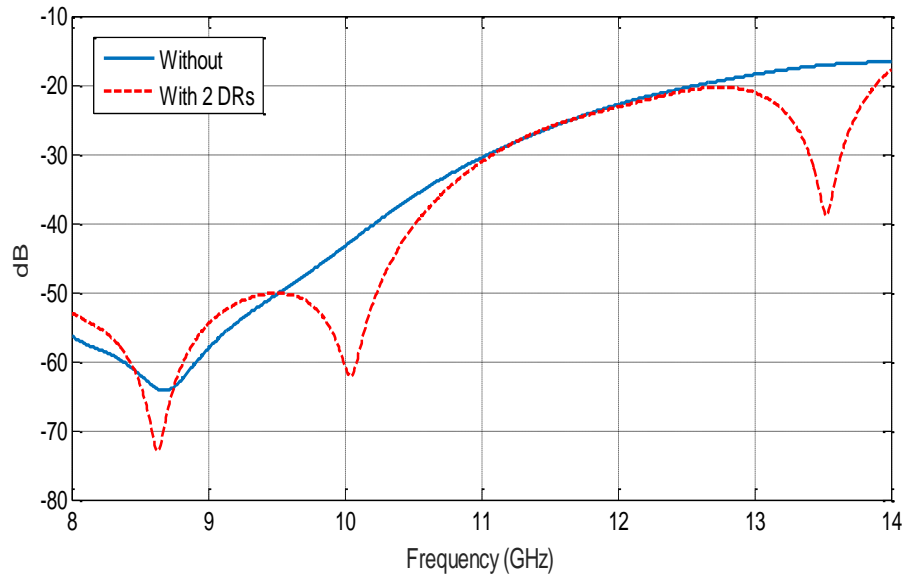


Figure 4.8 Isolation of multihole coupler with and without two dielectric resonators.

After the insufficient performance of the structure with two dielectric resonators, it is investigated whether the increase in the number of dielectric resonators can give better results or not. For this purpose, three dielectric resonators instead of two are placed between isolated port and holes as shown in Figure 4.9, and the simulations are repeated.

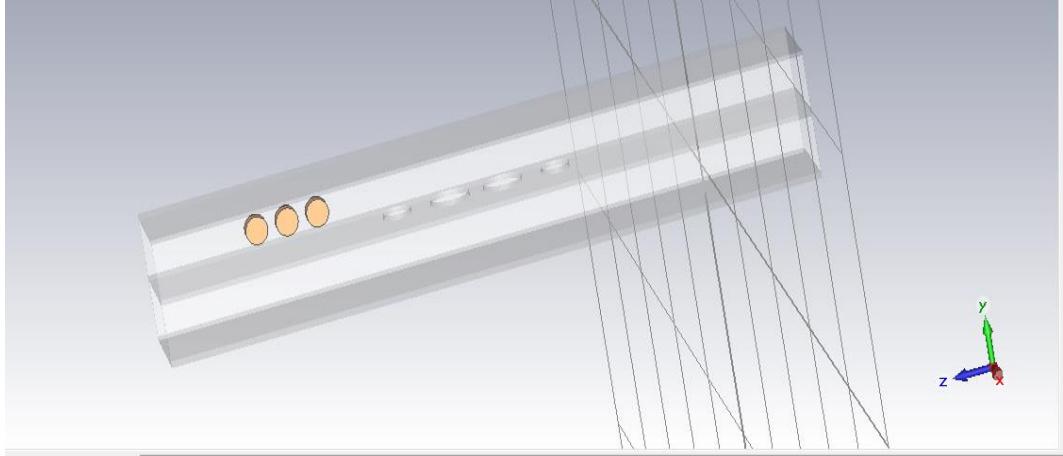


Figure 4.9 Simulation view of four-hole coupler with three dielectric resonators.

In the initial simulations of this structure, the distance in the z-axis between rightmost point of the resonator array and leftmost point of the hole array is selected as 16 mm. The length of hole array is fixed to 36.52 mm, which is the value used in the previous simulations. The coupling and isolation responses for the structure in Figure 4.9 with 16 mm distance are shown in Figure 4.10 and Figure 4.11 (the ones with the green solid lines), respectively.

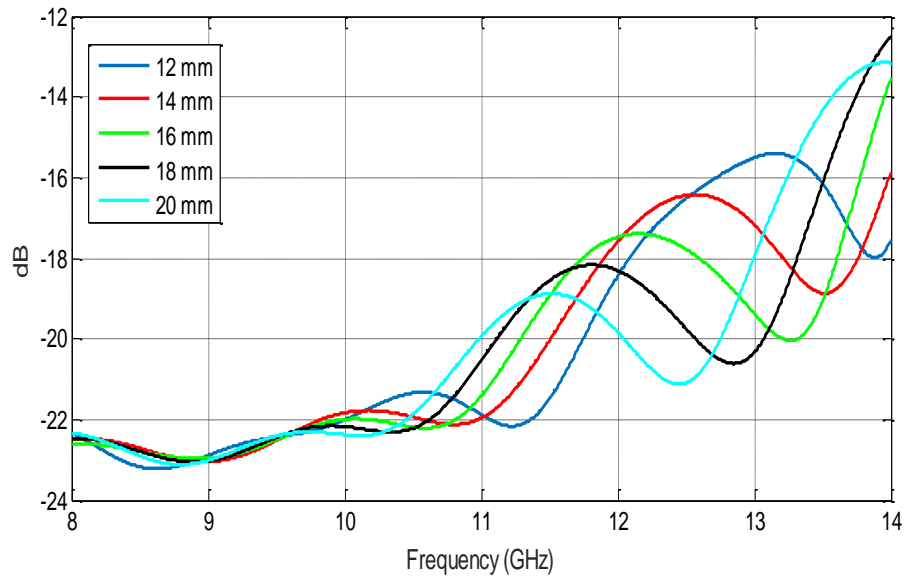


Figure 4.10 Coupling of multihole coupler with three dielectric resonators with different distances from holes.

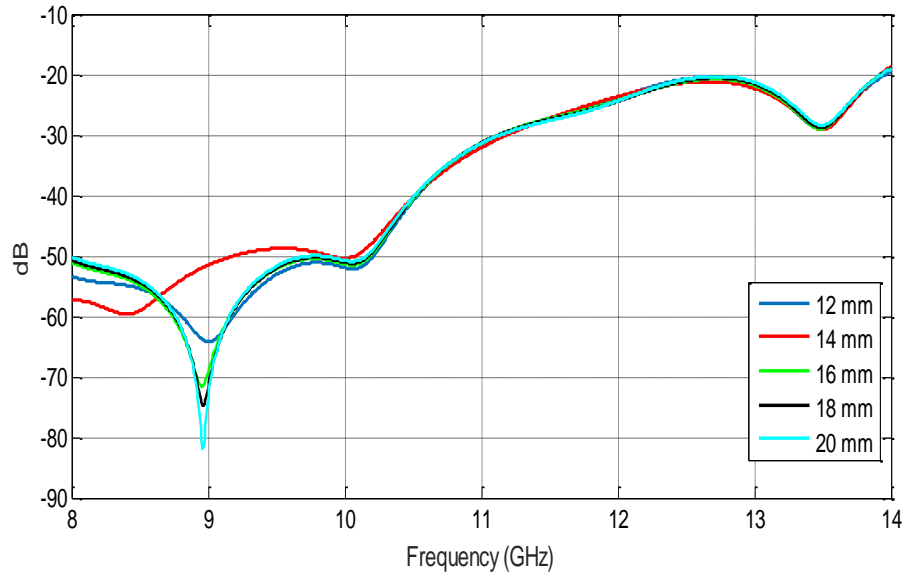


Figure 4.11 Isolation of multihole coupler with three dielectric resonators with different distances from holes.

The isolation results in Figure 4.11 are so similar to the ones in Figure 4.6, which belongs to the case of two dielectric resonators. The structure with three dielectric resonators still has isolation above 20 dB along the overall band (8-14 GHz), around 30 dB isolation at 13.5 GHz. Therefore, significant improvement is still observed in terms of isolation performance of the coupler with three dielectric resonators as compared to the case of two dielectric resonators. Besides, a remarkable enhancement can be noticed when the coupling response in Figure 4.10 is considered. It can be observed from these results that the coupling is above almost 18 dB in the frequency band of 8-13.5 GHz (nearly all of the overall band), and it is 20 dB (which is the desired value in the original design) at the frequency of about 13.27 GHz. When the frequency of 13.25-13.5 GHz is considered, the structure has the coupling of 18-20 dB and a minimum isolation of 25 dB. These values can be considered sufficient for the proper working of the coupler; therefore, the coupler can be said to have another operating frequency band of 13.25-13.5 GHz as well as 8-10 GHz. So, the metamaterial structure with three dielectric resonators adds a new band (multi-band) to the coupler, and improves the performance.

When the frequency having the highest coupling in the new band (13.27 GHz) is considered, coupling and isolation values in the case without metamaterial are close to each other and almost equal to 16 dB at this frequency. However, the coupling value increases to 20 dB with the addition of the metamaterial structure. The performance increase specific to this frequency can be explained as follows.

For the coupler without dielectric resonators, the coupling port has the wave contributions coming from the waves coupled through the holes and propagating towards the coupling port. The total contribution of these waves is around 16 dB for the case without dielectric resonators. However, when the dielectric resonators are placed between the isolation port and holes, the coupling port has now two main contributions. The first contribution includes the waves described above. The second contributions come from the waves, which are first coupled through the holes and propagates through the isolation port, then reflect from the metamaterial structure and go towards the coupling port. Since both waves have the magnitudes close to each other at 13.27 GHz, a reduction in the magnitude of total wave (so the increase in the coupling value) can be observed if the waves of both contributions are interfered as out of phase (180° phase shift). At 13.27 GHz, the corresponding guided wavelength (λ_g) for the dominant TE_{10} mode is calculated as about 26 mm inside the rectangular waveguide. When the 16 mm distance between DRs and holes, and the 36.52 mm length of the hole array are added, it gives the total length of 52.52 mm. This total length corresponds to almost $2\lambda_g$ in space. Since the waves in the second contribution go towards the isolation port and reflects back the coupling port, they move an additional distance of $4\lambda_g$ in space as compared to the waves in the first contribution (the waves directly going to coupling port). However, a space shift of $4\lambda_g$ results in 1440° phase shift, or equivalently 0° phase shift (in phase). So, actually the waves of both contributions should be interfered as in phase at 13.27 GHz, and the coupling value should decrease. But, this explanation is valid if the structure with dielectric resonators making the incoming waves to the isolation port reflect back to the coupling port is a right-handed metamaterial. However, since the array of dielectric resonators exhibits metamaterial characteristics at 13.27 GHz, this left-handed behaviour causes a 180° phase shift by making the electric field in the

opposite direction as compared to electric field of right-handed wave (see Figure 2.2). Consequently, this additional 180° phase shift makes the waves of both contributions to be added destructively as out of phase.

After it is found that the frequency with the minimum coupling value in the new frequency band (13.27 GHz) has a direct relationship with the total length of distance from resonators to hole array and length of hole array, it is analyzed whether this frequency can be shifted by varying the total length. In the simulations, since the length of the hole array is fixed to a constant value of 36.52 mm, the total length is changed by varying the distance from resonators to hole array rather than 16 mm. So, the total length becomes different than 52.52 mm. For this purpose, the simulations are carried out for the distances of 12, 14, 18 and 20 mm by giving total length of 48.52, 50.52, 54.52 and 56.52 mm, respectively. The performances of coupling and isolation of the multihole coupler with these distances are shown in Figure 4.10 and Figure 4.11, respectively along with the results of 16 mm.

When the results in Figure 4.10 are examined, it can be observed that the mentioned frequency becomes about 13.9 GHz for 12 mm distance, 13.5 GHz for 14 mm distance, 12.85 GHz for 18 mm distance and 12.45 GHz for 20 mm distance. The corresponding guided wavelengths at these frequencies are found to be 24.5 mm, 25.4 mm, 27.1 mm and 28.3 mm. When the total lengths (the sum of distance from resonators to hole array and length of hole array) for these cases are considered, which are 48.52 mm, 50.52 mm, 54.52 mm, and 56.52 mm, they again correspond to almost $2\lambda_g$ in length at the mentioned frequencies of 13.9 GHz, 13.5 GHz, 12.85 GHz and 12.45 GHz. Therefore, the explanation given above for the case of 16 mm is also verified for the other distances. Besides, an important result is revealed that the frequency with the minimum coupling can be adjusted by varying the distance of dielectric resonators to the hole array.

When the results about the isolation in Figure 4.11 are investigated, there is no significant change in the performance of the isolation with the respect to the change in the distance from dielectric resonators to the hole array.

When the responses in Figure 4.10 and Figure 4.11 are handled together, the case with 14 mm distance can be interpreted as giving the best performance among all cases. This is because the coupling and isolation are above 16 dB and 20 dB in the overall frequency band (8-14 GHz), which is not satisfied in the other cases. Besides, these values are above 18 dB and 25 dB, respectively, for the frequency band of 13.2-13.75 GHz. Therefore, a new operating frequency band can be again said to be appended to the coupler, which results in multi-band characteristics. This new frequency band (13.2-13.75 GHz) is wider as compared to the case of 16 mm (13.25-13.5 GHz). Therefore, again it can be concluded that the new operating frequency band can be reconfigured by adjusting the distance from resonators to the holes.

In this section, final analysis and simulations are done for the different number of dielectric resonators used in the structure in order to observe the effect of number of dielectric resonators on coupling and isolation performance. In these simulations, the distance from resonators to the holes is kept as 16 mm, and the number of dielectric resonators is increased along the isolation port. The responses are given in Figure 4.12 and Figure 4.13 for the coupling and isolation, respectively.

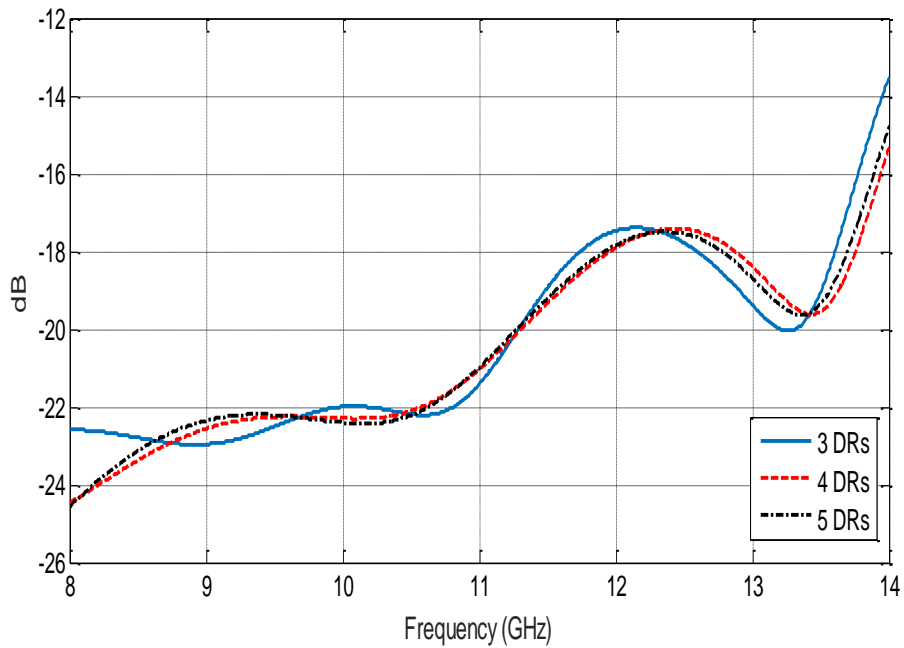


Figure 4.12 Coupling of multihole coupler with different number of dielectric resonators.

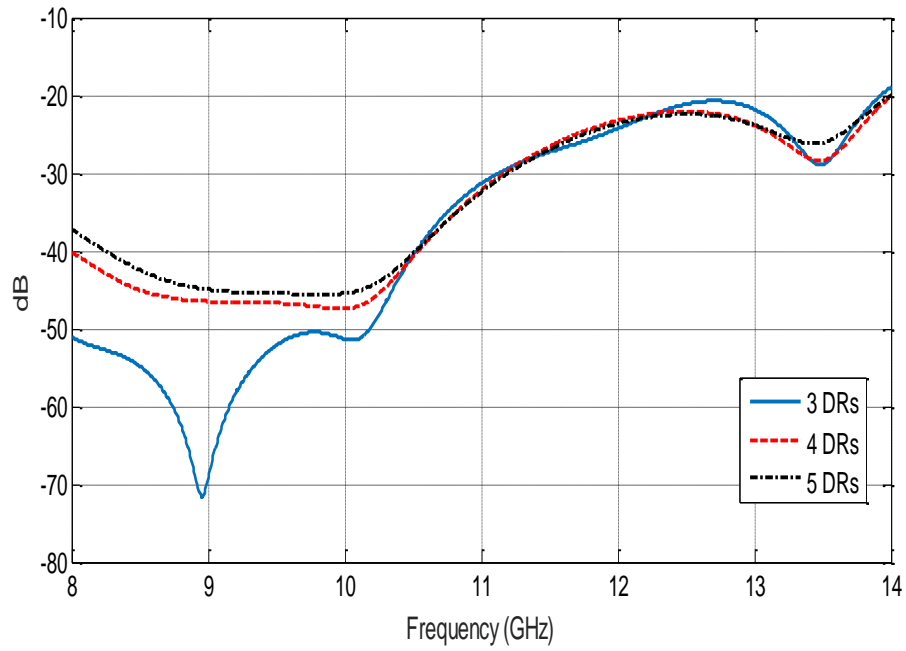


Figure 4.13 Isolation of multihole coupler with different number of dielectric resonators

According to the results in Figure 4.12 for the coupling response, the number of dielectric resonators has very small effect on the coupling performance. The increase in the number of dielectric resonators just slightly shifts the frequency with minimum coupling without any significant increase in the band with minimum 18 dB. On the other hand, the increase in the number of dielectric resonators results in an enhancement in the isolation performance. The isolation value becomes minimum 25 dB over nearly all of the band when four or five dielectric resonators are used, which is minimum 20 dB in the case of three dielectric resonators. When the threshold values of minimum 18 dB coupling and 25 dB isolation are considered, the cases with four and five dielectric resonators satisfy these values over the frequency band of 13-13.75 GHz. So, when compared with the case of three dielectric resonators having the new operating frequency band of 13.25-13.5 GHz, the increase in the number of dielectric resonators causes a remarkable increase in the bandwidth of the added frequency band as expected.

CHAPTER FIVE

CONCLUSION

In this thesis, the metamaterial characteristics of an array consisting of more than one dielectric resonators for different waveguide geometries and wave excitations is examined. Then, an implementation of the proposed metamaterial is used for a multi-hole rectangular waveguide coupler.

In order to observe the metamaterial behaviour of the dielectric resonator array, two cylindrical dielectrics with very high dielectric constant value ($\epsilon_r = 38$) are first put into WR90 rectangular waveguide (22.86 mm by 10.16 mm), which operates in X-band with the dominant TE_{10} mode. The dielectric resonators are positioned very close to each other to provide double resonance effect, which is a significant indicator about the metamaterial characteristics. The reflection (S_{11}) and the transmission (S_{21}) coefficients of the structure are first obtained from both the simulations and the measurements in the frequency range 8-14 GHz. Especially, when the transmission coefficients are considered, the structure exhibits double resonance effect at the frequency bands around 10 GHz and 13.5 GHz. Then, by performing the steps of a special method of effective medium parameter extraction, which are de-embedding and retrieval techniques, the effective permittivity and permeability values are calculated. From these calculations, it is found that the structure behaves as a metamaterial at the double resonance frequencies of 10 GHz and 13.5 GHz by giving negative permittivity and permeability (double negative-DNG) at these frequencies. Afterwards, in order to examine the metamaterial behaviour of the structure for different geometries and wave excitations, the rectangular waveguide in which the dielectric resonators is replaced by a parallel-plate waveguide with the dimension of 22.86 mm same as rectangular waveguide. Therefore, the wave excitation is converted from TE_{10} mode to TEM mode. When a similar calculations and analysis are done for the parallel-plate waveguide structure, it is shown that DNG frequencies with negative permittivity and permeability slightly shifts as compared to those of rectangular waveguide. The variation of metamaterial

characteristics of the proposed dielectric resonator array is shown to be highly insensitive to the different waveguide structures and wave excitations.

In the second part of the thesis, the proposed metamaterial structure with dielectric resonators is used to improve the performance of a conventional waveguide directional coupler. For this purpose, a four-hole WR90 rectangular waveguide coupler is designed to give about 20 dB coupling and minimum 40 dB isolation for the frequency band of 8-10 GHz, which coincides with one of the DNG frequencies of the proposed metamaterial structure. Then, the array with two dielectric resonators is inserted between isolation port and holes in order to see any improvement in the performances of coupling and isolation. The simulations are again done for 8-14 GHz. From the simulation results of the coupling and the isolation of the new coupler, it is obtained that although the metamaterial provides a reasonable improvement in the isolation at the frequency band of 13.5 GHz, which is the other DNG frequency of the proposed metamaterial, the improvement in coupling at this frequency is not adequate. To observe the effects of element number in the array, the number of dielectric resonators is increased to three, and similar simulations are repeated. These new simulations result in valuable improvements in the coupling and isolation by satisfying minimum 18 dB coupling and 25 dB isolation at the frequency band of 13.25-13.5 GHz. The material structure with three dielectric resonators provides a new operating frequency band to the conventional coupler at one of DNG frequencies of the metamaterial. Besides, when the frequency with maximum coupling within this new frequency band is considered, a relation between this frequency and distance between resonators and holes is found. By using this relation, it is shown that the mentioned frequency can be varied by adjusting the distance properly although the change in the distance does not affect the isolation performance significantly. Therefore, the new operating frequency band can be reconfigured with the proper arrangement of the dielectric resonators. For example, it is demonstrated with the additional simulations that the frequency band becomes 13.2-13.75 GHz when the distance changes from 16 mm to 14 mm where the case of 16 mm has 13.25-13.5 GHz frequency band. As a final analysis, the effect of the number of dielectric resonators on the performance of the coupler is investigated, and

the simulations with four and five dielectric resonators are realized. These simulations reveal that the increase in the number of dielectric resonators widens the bandwidth of the new frequency band, i.e. the coupler begins to operate between 13 GHz and 13.75 for the cases of four and five dielectric resonators.

Although the frequency with maximum coupling on the new band can be arranged to be far away from 13.5 GHz by changing the mentioned distance (for instance, it is 12.85 GHz for the case of 20 mm), the frequency having maximum isolation on the new band is almost independent from the distance, and only depends on the DNG frequency of the proposed metamaterial structure. Therefore, when both the coupling and the isolation of the coupler are considered together, the change in the distance can only make small frequency shifts or increase the bandwidth around 13.5 GHz. However, if a significant change is possible on DNG frequency of the metamaterial structure, the frequency having maximum isolation on the new band can be changed. Consequently, with the suitable arrangement of the mentioned distance, the new operating frequency band can be shifted to any frequency region, which is not necessarily around 13.5 GHz. Therefore, as a future work, the effects of parameters such as the distance between the dielectric resonators, the dimensions of the cylinders and the dielectric constant on the DNG frequencies of the proposed metamaterial can be examined, and it can be analyzed how these DNG frequencies change with respect to these parameters. Concluding that, the DNG frequencies of the proposed metamaterial can be controlled with these parameters, and the new frequency band of the coupler can be reconfigured.

REFERENCES

- Aydın, K., Bulu, I., & Ozbay, E. (2007). Subwavelength resolution with a negative-index metamaterial superlens. *Applied Physics Letters*, 90, 254102.
- Aydın, K., & Ozbay, E. (2007). Capacitor-loaded split ring resonators at tunable metamaterial components. *Journal of Applied Physics*, 101, 024911.
- Bayatpur, F. (2009). *Metamaterial-inspired frequency-selective surface*. Phd Thesis, The University of Michigan, USA.
- Bethe, H. A. (1944). Theory of diffraction by small holes. *Physical Review Letters*, 66, 163.
- Chen, F., Wang, X., & Semouchkina, E. (2011). Simulation and experimental studies of dielectric resonator arrays for designing metamaterials. *IEEE International Symposium on Antennas & Propagation*, 2936-2939.
- Chen, P. Y., & Alu, A. (2010). Sub-wavelength elliptical patch antenna loaded with μ -negative metamaterials. *IEEE Transactions on Antennas & Propagation*, 58(9), 2909-2919.
- Dong, Y., & Itoh, T. (2012). Metamaterial-based antennas. *Proceeding of the IEEE*, 100(7), 2271-2285.
- Ekmekçi, E. (2010). *Design, fabrication and characterization of novel metamaterials in microwave and terahertz regions: multi-band, frequency-tunable and miniaturized structures*. Phd Thesis, Middle East Technical University, Ankara.
- Ekmekçi, E., & Turhan-Sayan, G. (2009). Comparative investigation of resonance characteristics and electrical size of the double-sided SRR, BC-SRR and

- conventional SRR type metamaterials for varying substrate parameters. *Progress in Electromagnetic Research B*, 12, 35-62.
- Eleftheriades, G. V. (2004). Negative-refractive-index transmission line metamaterials and enabling microwave devices. *Antennas and propagation society international Symposium*, 2, 1399-1402.
- Engheta, N., & Ziolkowski, R.W. (2006). *Metamaterials physics and engineering explorations*. IEEE Press.
- Garcia-Garcia, J., Martin, F., Baena, J. D., Marques, R., & Jelinek, L. (2005). On the resonance and polarizabilities of split ring resonators. *Journal of Applied Physics*, 98, 033103.
- Ghodgaonkar, D. K., Varadan, V. V., & Varadan, V. K. (1990). Free-space measurement of complex permittivity and complex permeability of magnetic materials at microwave frequencies. *IEEE Transactions on Instrumentation and Measurement*, 39(2), 387-394.
- Jiang, D., Xu, Y. -H., Xu, R. -M., & Lin, W.-G. (2013). Implementation of a novel broadband microstrip metamaterial power divider. *Journal of Electromagnetic Waves and Applications*, 27(5), 591-598.
- Kim, I. K., & Varadan, V. V (2010). Electrically small, millimeter wave dual-band meta-resonator antennas. *IEEE Transactions on Antennas & Propagation*, 58(11), 3458-3463.
- Koschny, T., Kafesaki, M., Economou, E. N., & Soukoulis, C. M. (2004). Effective medium theory of left-handed metaterials. *Physical Review Letters*, 93.
- Ludwig, R., & Bretchko, P. (2000). *RF circuit design theory and application*, Upper Saddle River, New Jersey, USA: Prentice-Hall.

- Majedi, M. S., & Attari, A. R. (2013). A compact and broadband metamaterial-inspired antenna. *IEEE Antennas and Wireless Propagation Letters*, 12, 345-348.
- Markos, P., & Soukoulis, C. M. (2001). Numerical studies of left-handed materials and arrays of split ring resonators. *Physical Review E*, 65.
- Oraizi, H., & Afsahi, M. (2009). Design of metamaterial multilayer structures as frequency selective surfaces. *Progress in Electromagnetics Research C*, 6, 115-126.
- Pendry, J. B. (2000). Negative refraction makes a perfect lens. *Physical Review Letters*, 85(18), 3966-3969.
- Pendry, J. B. (2007). Metamaterials and the control of electromagnetics fields. *Conference on Coherence and Quantum Optics*. Paper CMB2.
- Pendry, J. B., Holden, A.J., Robbins, D. J., & Stewart, W. J. (1999). Low frequency plasmons in thin wire structure. *Journal of Physics: Condensed Matter*, 10(22).
- Pendry, J. B., Holden, A. J., Robbins, D. J., & Stewart, W.J. (1999). Magnetism from conductors and enhanced nonlinear phenomena. *IEEE Transactions on. Microwave Theory & Techniques*, 47(11), 2075-2084.
- Pendry, J. B., Holden, A. J., Stewart, W. J., & Youngs, I. (1996). Extremely low frequency plasmons in metallic mesostructures. *Physical Review Letters*, 76(25), 4773-4776.
- Pendry, J. B., Schurig, D., & Smith, D. R. (2006). Controlling electromagnetic fields. *Science*, 312, 1780-1782.

- Plourde, J. K., & Ren, C. L. (1981). Application of dielectric resonators in microwave components. *IEEE Transactions on Microwave Theory & Techniques*, 29(8), 754-768.
- Pozar, D. M. (2012). *Microwave engineering*, (4th ed.), Hoboken, NJ, USA: John-Wiley Sons Inc.
- Sahu, B., Tripathi, P., Singh, R., & Singh, S. P. (2013). Simulation study of dielectric resonator antennas with metamaterial for improvement of bandwidth and gain. *Microwave and RF Conference, 2013 IEEE MTT-S International*, 1-4.
- Semouchkina, E., Werner, D. H., Semouchkin, G., & Pantano, C. (2010). An infrared invisibility cloak composed of glass. *Applied Physics Letters*, 96, 233503.
- Smith, D. R., & Kroll, N. (2000). Negative refractive index in left-handed materials. *Physical Review Letters*, 85(14), 2933-2936.
- Smith, D. R., & Larauche, S. (2010). A retrieval method for nonlinear metamaterials. *Optics Communications*, 283, 1621-1627.
- Smith, D. R., Padilla, W.J., Vier, D. C., Nemat-Nasser, S. C., & Schultz, S. (2000). Composite medium with simultaneously negative permeability and permittivity. *Physical Review Letters*, 84(18), 4184-4187.
- Smith, D. R., & Pendry, J. B. (2004). Reversing light with negative refraction. *American Institute of Physics*, 37-43.
- Smith, D. R., Vier, D. C., Koschny, Th., & Soukoulis, M. (2005). Electromagnetic parameter retrieval from inhomogeneous metamaterials. *Physical Review E*, 71.
- Ueda, T., Lai, A., & Itoh, T. (2007). Demonstration of negative refraction in a cutoff parallel-plate waveguide loaded with two-dimensional lattice of dielectric

- resonators. *IEEE Transactions on Microwave Theory & Techniques*, 55, 1280–1287.
- Ueda, T., Lai, A., & Itoh, T. (n.d) *Dielectric resonator-based left handed materials: Guided wave*. Retrieved July 20, 2015 from <http://www.ee.ucla.edu.mwlab>.
- Ueda, T., Michishita, N., Akiyama, M., & Itoh, T. (2010). Anisotropic 3-D composite right/left-handed metamaterial structures using dielectric resonators and conductive mesh plates. *IEEE Transactions on Microwave Theory & Techniques*, 58, 1766 -1773.
- Ung, B. (2009). Metamaterials: A metareview. *Ecole Polytechnique de Montreal*, Canada.
- Upadhyaya, T.K., Kosta, S. P., Jyoti, R., & Palandoken, M. (2014). Negative refractive index material-inspired 90-deg electrically tilted ultra wideband resonator. *Optical Engineering*, 53(10), 107104.
- Veselago, V. G. (1968). The electrodynamics of substances with simultaneously negative values of ϵ and μ . *Soviet Physics Uspekhi*, 10(4), 509-514.
- Wang, J., Qu, S., Ma, H., Hu, J., Yang, Y., & Wu, X. (2009). A dielectric resonator based route to left handed metamaterials. *Progress in Electromagnetic Research B*, 13, 133-150.
- Weir, W. B. (1974). Automatic measurement of complex dielectric constant and permeability at microwave frequencies. *Proceedings of the IEEE*, 62(1), 33-36.
- Withayachumnankul, W., & Abbott, D. (2009). Metamaterials in the terahertz regime. *IEEE Photonics Journal*, 1(2), 99-118.

Wolf, E., & Habashy, T. (2007). Invisible bodies and uniqueness of the inverse scattering problem. *Journal of Modern Optics*, 40(5), 785-792.

Xiong, H., Hong, J.S., Tan, M.T., & Li, B. (2013). Compact microstrip antenna with metamaterial for wideband applications. *Turkish Journal of Electrical Engineering & Computer Sciences*, 2233-2238.

Yang, J. J., Huang, M., Tang, H., Zeng, J., & Dong, L. (2013). Metamaterial sensors. *International Journal of Antennas and Propagation*. 2013, 637270.

APPENDICES

APPENDIX-1: SAMPLE MATLAB CODES FOR RETRIEVAL TECHNIQUE

%% COMPLEX PERMITTIVITY and PERMEABILITY CONSTANT
CALCULATION %%%

%% for rectangular waveguide

```
close all
clear all
%%%load measured S11 and S21 data %%%%%%%%%%
load s11_meta.mat;
load s21_meta.mat;
load f.mat
S11=s11_meta;
S21=s21_meta;
%s11_8;
%s21_8;

a=22.86*1e-3; %width of waveguide

d=5*1e-3+2e-3; % distance between DRs

%Equation 6
xx=((S11).^2)-((S21).^2)+1)./(2*S11);
%Equation 5
rr1=xx+sqrt((xx.^2)-1); % +
rr2=xx-sqrt((xx.^2)-1); % -

for i=1:length(S11)
    if abs(rr1(i))<1
        rr(i)=rr1(i);
    else
        rr(i)=rr2(i);
    end
end

%rr=rr.';

%Equation 7
pp1=((S11.^2)-(S21.^2)-rr)./(1-((S11-S21).*rr));

%Equation 8
aa1=-(((1/(2*pi*d))*(log(1./pp1) - j*2*pi*0    )).^2);
```

```

vv1=sqrt(1./aa1);

%Equation 9
lambda0=((3E8)./f)';
mur1=(1.+rr)./(vv1.*(1-rr).*sqrt(((1./lambda0).^2)-(((1/(2*a))^2)))));

% Equation 8'den e_r bulma
epsr1=((lambda0.^2).*(aa1+((1/(2*a))^2)))./mur1;

figure
plot(f,real(epsr1));
hold
plot(f,imag(epsr1),'r');
legend('\epsilon_r{eff}','\epsilon_i{eff}');
grid

figure
plot(f,real(mur1));
hold
plot(f,imag(mur1),'r');
legend('\mu_r{eff}','\mu_i{eff}');
grid

% lam=1./real(1./vv1);
% figure
% plot(f,lam)

%%%%%%%%%%%%%%%%%%%%%%%%%%%%%%%%%%%%%%%%%%%%%%%%%%%%%%%%%%%%%%%%%%%%%%%%

%% for parallel plate waveguide
close all
clear all
%%%load measured S11 and S21 data %%%%%%%%%
load freespace_s11_meta.mat;
load freespace_s21_meta.mat;
load f.mat
S11=s11_meta;
S21=s21_meta;
%s11_8;
%s21_8;
f0=f;
%a=34.8*1e-3; %width of waveguide
c=3e8;
d=5*1e-3+2e-3; % distance between DRs

```

```

K=(S11.^2-S21.^2+1)./(2*S11);

Ra=K+sqrt(K.^2-1);
Re=K-sqrt(K.^2-1);

[M N]=size(f0);

for m=1:M,
    if abs(Ra(1,m))>1
        Ra(1,m)=Re(1,m);
    else
        Ra(1,m)=Ra(1,m);
    end
end

R=Ra;

T=(S11+S21-R)./(1-(S11+S21).*R);

k=-2;
gama=(log(1./(abs(T)))+(i*(2*pi*k-angle(T))))/d;
gama0=i*2*pi*f0/c;
eps=(gama./gama0).*((1-R)./(1+R));
mue=(gama./gama0).*((1+R)./(1-R));

figure
plot(f0*1e-9,real(eps));
hold
plot(f0*1e-9,(1*imag(eps)), 'r');
legend('\epsilon_r{eff}', '\epsilon_i{eff}');
xlabel('Frequency (GHz)');
ylabel('Effective Permittivity');
grid

figure
plot(f0*1e-9,real(mue));
hold
plot(f0*1e-9,(1*imag(mue)), 'r');
xlabel('Frequency (GHz)');
ylabel('Effective Permeability');
legend('\mu_r{eff}', '\mu_i{eff}');
grid

```

APPENDIX-2: CALCULATIONS FOR FOUR HOLE WAVEGUIDE DIRECTIONAL COUPLER

In this four-hole Chebyshev waveguide directional coupler designed, it is aimed to obtain 20 dB coupling and minimum 40 dB directivity at the center frequency $f_0 = 9$ GHz. The waveguide used in the design is standard WR-90 with the dimensions of $a = 22.86$ mm and $b = 10.16$ mm. The holes are located at $s = a/4 = 5.715$ mm away from the edge wall.

For a Chebyshev design with the even number of holes, the radii of the holes can be found from the following equation [42]

$$2 \sum_{n=0}^{(N-1)/2} r_n^3 \cos(N-2n)\theta = k |T_N(\sec \theta_m \cos \theta)| \quad (\text{A2.1})$$

where $N = (\# \text{ of holes} - 1)$, r_n values for $n = 0, 1, \dots, N-1$ are the radii of the holes, which is symmetric such that $r_n = r_{N-n}$. Here, T_N is the Chebyshev function with the order of N ; k and θ_m are some constants to be determined. Since $N = 4 - 1 = 3$ in our design, the equation (A2.1) is modified by using Chebyshev expansion of T_3 as

$$2(r_0^3 \cos 3\theta + r_1^3 \cos \theta) = k [\sec^3 \theta_m (\cos 3\theta + 3 \cos \theta) - 3 \sec \theta_m \cos \theta] \quad (\text{A2.2})$$

By equating the coefficients of terms of $\cos(3\theta)$ and $\cos(\theta)$ in equation (A2.2), the radii can be solved by also using the symmetric structure as

$$2r_0^3 = 2r_3^3 = k \sec^3 \theta_m \quad (\text{A2.3})$$

$$2r_1^3 = 2r_2^3 = 3k (\sec^3 \theta_m - 3 \sec \theta_m) \quad (\text{A2.4})$$

The constant θ_m in (A2.3) and (A2.4) is calculated from the following equation [42].

$$D_{\min}(\text{dB}) = 20 \log T_N (\sec \theta_m) \quad (\text{A2.5})$$

where $D_{\min}(\text{dB})$ is the minimum directivity in dB, which is 40 dB in our example. Therefore, it can be evaluated from (A2.5) that

$$\begin{aligned} 40 &= 20 \log T_3 (\sec \theta_m) \Rightarrow 100 = T_3 (\sec \theta_m) = \cosh \left[3 \cosh^{-1} (\sec \theta_m) \right] \\ \sec \theta_m &= 3.01 \Rightarrow \theta_m = 70.6^\circ \end{aligned} \quad (\text{A2.6})$$

The other constant k can be calculated from the following equation as

$$C(\text{dB}) = -20 \log (|K_f|) - 20 \log k - D_{\min}(\text{dB}) \quad (\text{A2.7})$$

where $C(\text{dB})$ is the coupling in dB, which is 20 dB in our example, and K_f is the amplitude of the wave travelling through coupling port. From the small-aperture coupling theory, the equation for K_f is given as

$$|K_f| = \frac{2k_0}{3\eta_0 P_{10}} \left[\sin^2 \frac{\pi s}{a} - \frac{2\beta^2}{k_0^2} \left(\sin^2 \frac{\pi s}{a} + \frac{\pi^2}{\beta^2 a^2} \cos^2 \frac{\pi s}{a} \right) \right] \quad (\text{A2.8})$$

where $\eta_0 = 120\pi$ is the wave impedance of free space, and the other constants of k_0 (wavenumber in free space), P_{10} (power normalization constant) and β (phase constant of the propagating wave) are given as

$$k_0 = \frac{2\pi f_0}{c} = \frac{2\pi(9 \times 10^9)}{3 \times 10^8} = 188.5 \text{ rad / m} \quad (\text{A2.9})$$

$$P_{10} = \frac{ab}{\eta_0} \sqrt{1 - \left(\frac{3 \times 10^8}{2af_0} \right)^2} = 4.22 \times 10^{-7} \text{ m}^2 / \Omega \quad (\text{A2.10})$$

$$\beta = \sqrt{k_0^2 - \left(\frac{\pi}{a} \right)^2} = 129 \text{ rad / m} \quad (\text{A2.11})$$

By using the values in (A2.9)-(A2.11) and other constants, the amplitude in (A2.8) is calculated as $|K_f| = 3.953 \times 10^5$. Then by using (A2.7), the constant value of k is evaluated as

$$\begin{aligned} 20 &= -20\log(3.953 \times 10^5) - 20\log k - 40 \\ 20\log k &= -171.94 \Rightarrow k = 2.53 \times 10^{-9} \end{aligned} \quad (\text{A2.12})$$

Finally, the radii of the holes can be calculated by substituting $\theta_m = 70.6^\circ$ and $k = 2.53 \times 10^{-9}$ into the equations (A2.3) and (A2.4) such that

$$2r_0^3 = 2r_3^3 = (2.53 \times 10^{-9}) \sec^3(70.6^\circ) \Rightarrow r_0 = r_3 = 3.26 \text{ mm} \quad (\text{A2.13})$$

$$2r_1^3 = 2r_2^3 = 7.59 \times 10^{-9} (\sec^3(70.6^\circ) - 3\sec(70.6^\circ)) \Rightarrow r_1 = r_2 = 4.51 \text{ mm} \quad (\text{A2.14})$$